参观完气象局，你有什么感受？

强对流触发的决定性因子

上节课回顾

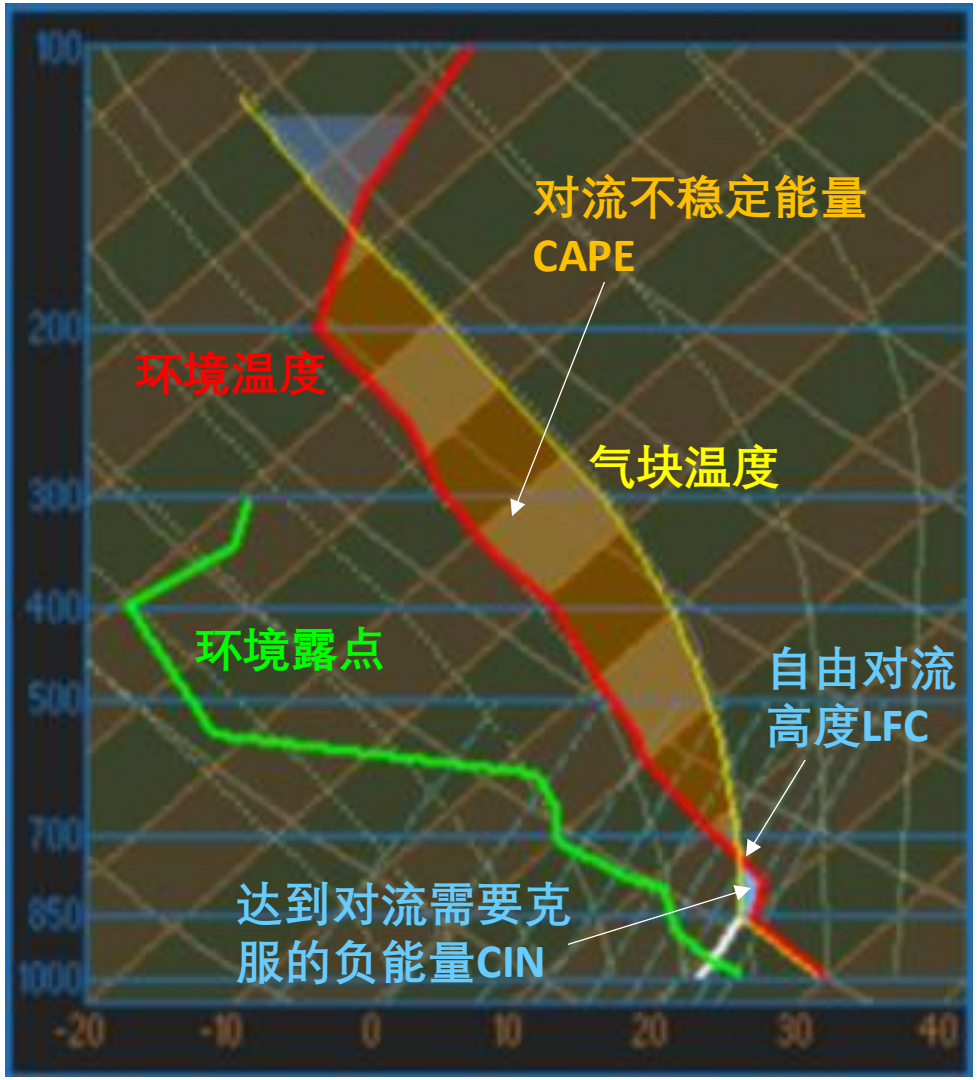

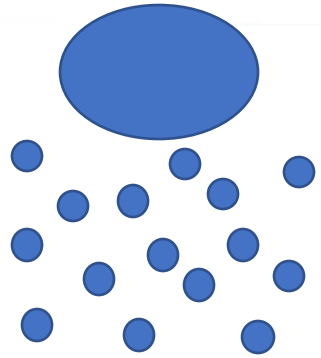

对流触发三大条件：

- **水汽**
- **不稳定能量**
- **抬升机制**

地基对流：地形、边界层辐合线（海陆锋、干线、边界层滚涡、阵风锋）

高架对流：边界层顶附近的抬升

(1）天气尺度系统的作用

上节课回顾

Prime the mesoscale environment

-- 减小CIN　-- 加厚低层湿层

1）环境减温率倾向方程 $\frac{\partial \gamma}{\partial t}$

$$c_p \frac{dT}{dt} - \alpha \frac{dp}{dt} = q$$

单位质量气块的加热率

$$\alpha \frac{dp}{dt} = \frac{1}{\rho} \frac{dp}{dz} \frac{dz}{dt} = -\frac{1}{\rho} \rho g \frac{dz}{dt} = -gw$$

$$c_p \left(\frac{\partial T}{\partial t} + \vec{v_h} \cdot \nabla_h T + w \frac{\partial T}{\partial z} \right) + gw = q$$

1）环境减温率倾向方程 $\frac{\partial\gamma}{\partial t}$

上节课回顾

$$-\frac{\partial q}{\partial z}=\mathrm{c_p}\left(\frac{\partial\gamma}{\partial t}-\frac{\partial\overrightarrow{\mathbf{v}_\mathrm{h}}}{\partial z}\cdot\nabla_\mathrm{h}T+w\frac{\partial\gamma}{\partial z}+\overrightarrow{\mathbf{v}_\mathrm{h}}\cdot\nabla_\mathrm{h}\gamma+\frac{\partial w}{\partial z}\gamma\right)-\mathrm{g}\frac{\partial w}{\partial z}$$

$$\frac{\partial\gamma}{\partial t}=-\overrightarrow{\mathbf{v}_\mathrm{h}}\cdot\nabla_\mathrm{h}\gamma-w\frac{\partial\gamma}{\partial z}+\frac{\partial\overrightarrow{\mathbf{v}_\mathrm{h}}}{\partial z}\cdot\nabla_\mathrm{h}T-\frac{\partial w}{\partial z}\gamma+\frac{\mathrm{g}}{\mathrm{c_p}}\frac{\partial w}{\partial z}-\frac{1}{\mathrm{c_p}}\frac{\partial q}{\partial z}$$

$$=-\overrightarrow{\mathbf{v}_\mathrm{h}}\cdot\nabla_\mathrm{h}\gamma-w\frac{\partial\gamma}{\partial z}+\frac{\partial\overrightarrow{\mathbf{v}_\mathrm{h}}}{\partial z}\cdot\nabla_\mathrm{h}T+\frac{\partial w}{\partial z}(\Gamma_\mathrm{d}-\gamma)-\frac{1}{\mathrm{c_p}}\frac{\partial q}{\partial z}$$

水平平流　垂直平流　拉伸项　差分非绝热加热

大尺度　10^{-7}　10^{-8}　10^{-8}　10^{-8}　10^{-9}

$$-\overrightarrow{\mathbf{v}_\mathrm{h}}\cdot\nabla_\mathrm{h}\gamma+\frac{\partial\overrightarrow{\mathbf{v}_\mathrm{h}}}{\partial z}\cdot\nabla_\mathrm{h}T=\overrightarrow{\mathbf{v}_\mathrm{h}}\cdot\nabla_\mathrm{h}\left(\frac{\partial T}{\partial z}\right)+\frac{\partial\overrightarrow{\mathbf{v}_\mathrm{h}}}{\partial z}\cdot\nabla_\mathrm{h}T=-\frac{\partial}{\partial z}(-\overrightarrow{\mathbf{v}_\mathrm{h}}\cdot\nabla_\mathrm{h}T)$$

差分温度平流

2）与$\frac{\partial \gamma}{\partial t}$无关的改变CAPE和CIN的过程

上节课回顾

上述Lapse rate的变化分析多为对中层Lapse rate的改变，可能会过分强调γ变化对CAPE和CIN变化的作用

- large-scale rising motion
- Moistening
- low-level warming

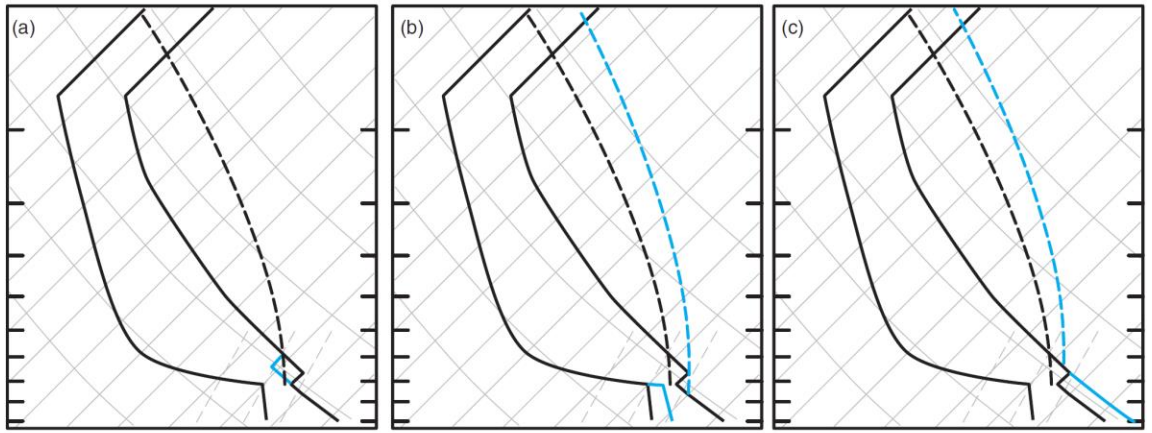

Figure 7.9 CIN can be reduced by (a) large-scale rising motion, (b) low-level moistening (e.g., moisture advection), and (c) low-level warming (e.g., insolation), despite the fact that the CIN modifications may not be accompanied by lapse rate changes, at least not over a significant depth. In (a)–(c), the isotherms and isentropes are solid gray lines, the constant mixing ratio lines are gray dashed lines, the sounding and trajectory taken by an air parcel lifted from the surface are solid and dashed black curves, respectively, and the modified sounding and parcel trajectory are blue solid and dashed curves, respectively. In (a), for clarity, only the temperature profile has been modified (the moisture profile has not been modified in accordance with the vertical motion that has been imposed in the layer of the capping inversion). Note that (b) and (c) are also accompanied by increases in CAPE. Conversely, CIN is augmented by large-scale descent, boundary layer cooling (although this would typically not occur without a concurrent stabilization of the lapse rate), and boundary layer drying (not shown).

(2) 中尺度系统的作用

上节课回顾

1）热力场的不均匀性

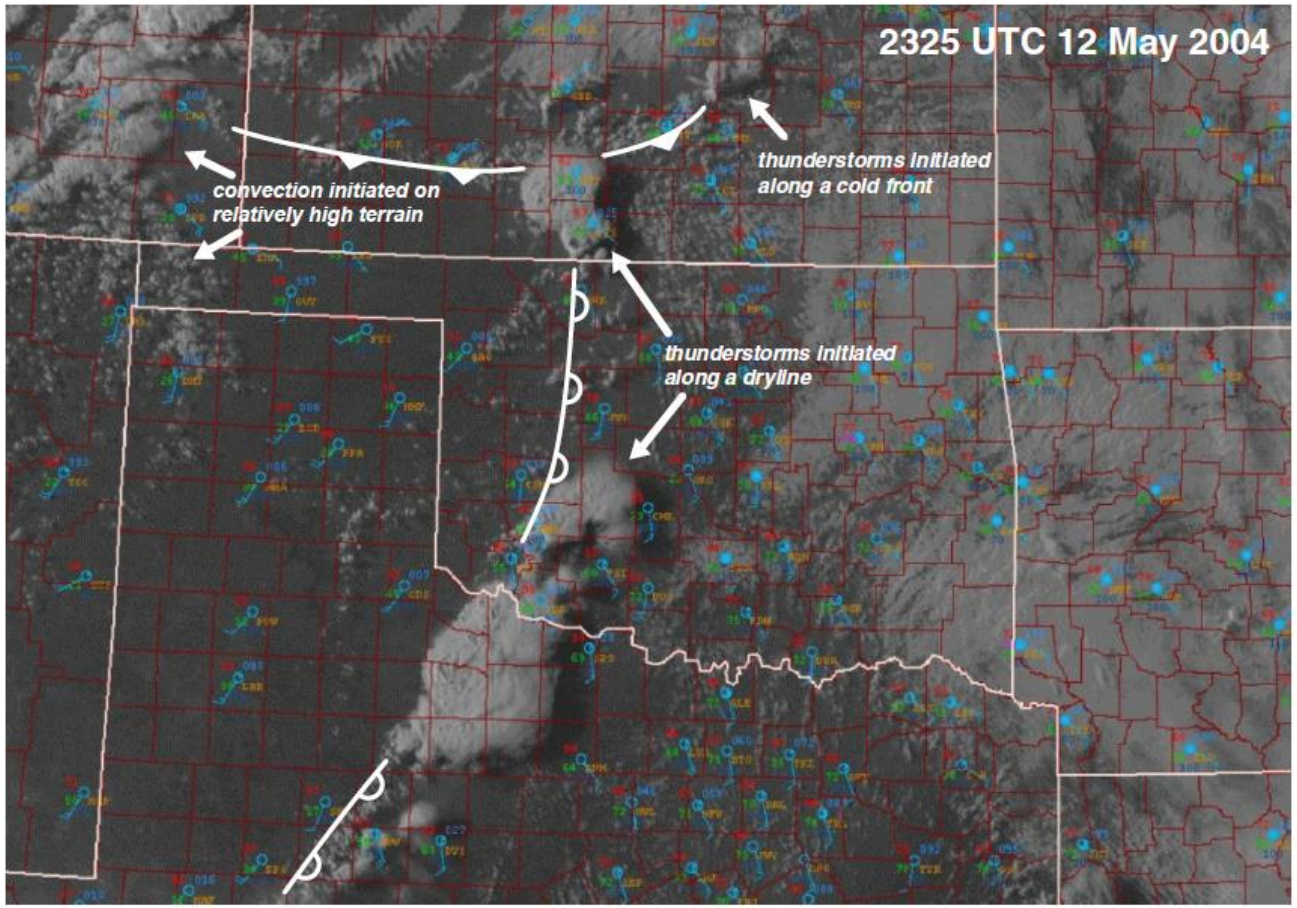

DMC仅在边界的某些部分发生

2）中尺度运动特征（动量）的不均匀性

上节课回顾

Convective rolls

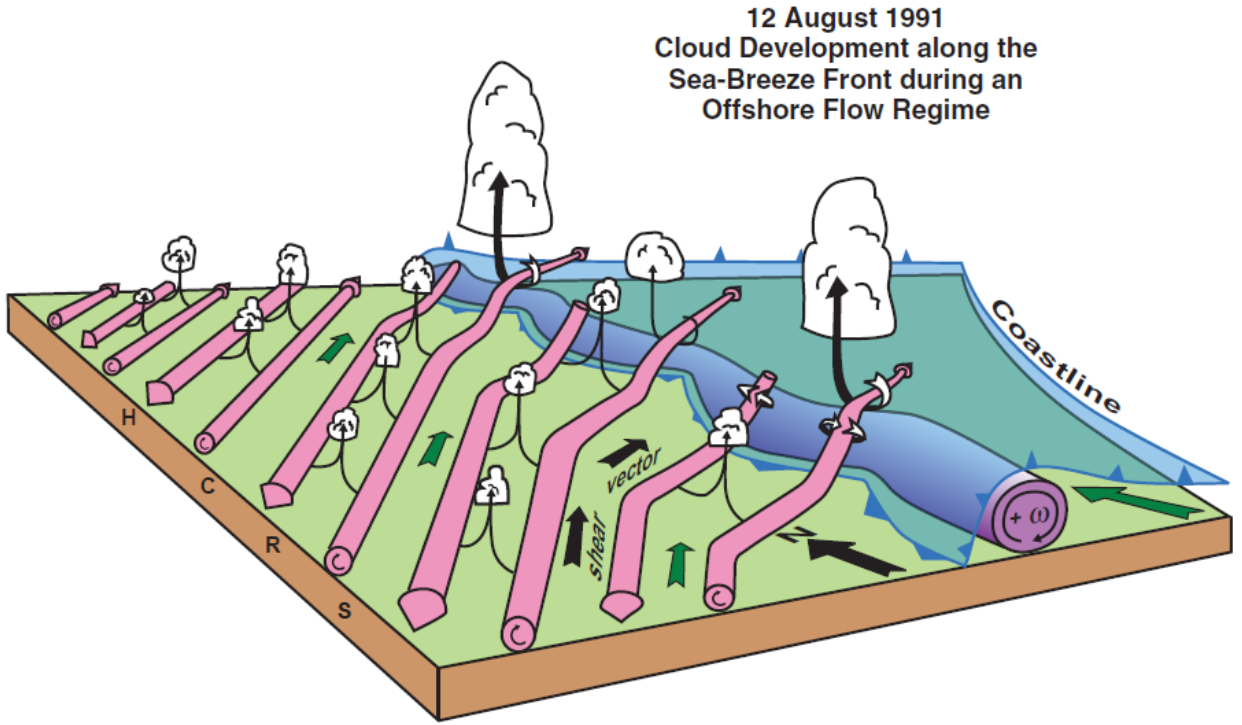

Figure 7.11 Schematic diagram showing the interaction between the sea-breeze front and horizontal convective rolls and how it related to cloud development on 12 August 1991 during the Convection and Precipitation/Electrification Experiment (CaPE). The sea-breeze front is delineated by the heavy blue barbed line. The circulation along the leading portion of the sea-breeze front is shaded purple. The horizontal vorticity vectors associated with the counter-rotating roll circulations are also shown, as are clouds along the horizontal convective rolls and at the intersection points along the front. The shear vector and low-level winds are indicated with black and green arrows, respectively. This is the same case as shown in Figure 5.33. (Adapted from Atkins and Wakimoto [1995].)

(3）DMC触发预报的误差分析

上节课回顾

- 完全没有CIN，DMC不发展
- 有很大的CIN，DMC仍发展
- 有CAPE，skew-T 估计的CIN被overcome (比如地面升温到了对流温度），但没有对流发展。

（4）有利于DMC发生的条件

上节课回顾

持续的低层辐合和较小的CIN

水汽的辐合：如何有利于CI的发生？

在持续性辐合的气团边界往往观测到较大的水汽混合比q_v

水汽的辐合能被解释为制造水汽混合比q_v的极值吗？

1) 水汽的水辐合本身并不能形成局地 q_v极大值

$$-\nabla\cdot(q_v\,\vec{\mathrm{v}}_\mathrm{h})>0$$

$$\frac{\partial q_v}{\partial t}=-\vec{\mathrm{v}}\cdot\nabla q_v-\mathrm{C}+\mathrm{E}=-\vec{\mathrm{v}}_\mathrm{h}\cdot\nabla_\mathrm{h}q_v-w\frac{\partial q_v}{\partial z}-\mathrm{C}+\mathrm{E}\quad①$$

在不考虑蒸发的情形下， 水汽的增加只能来自平流，而平流并不能产生局地极大值

Ch2.5 强对流的典型探空和触发环境


SZMG谈天说地
bilibili

2.9 与强对流相关的四类典型探空

Miller composite soundings (Col. R. Miller)，实际情况有可能会异于气候平均

(1) 第一类Miller探空，“Loaded Gun”

(水汽、不稳定度、CIN、SHR)

1) 特点：地面附近为一混合的湿层，湿层上面有一个稳定层（或逆温层），再上面是一个非常干的气层。

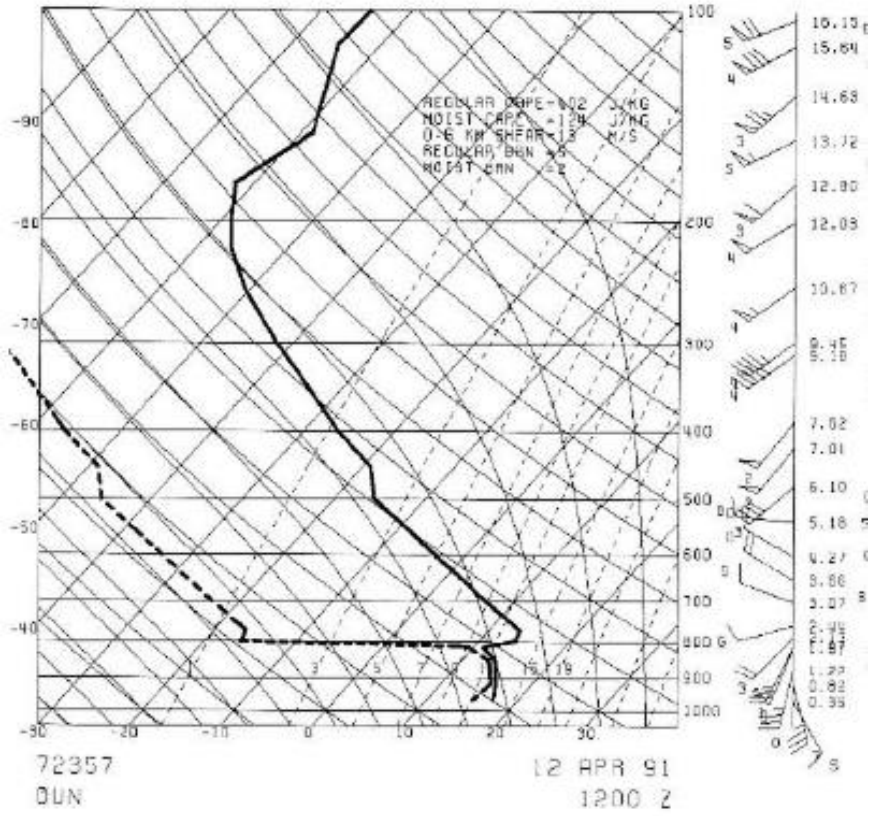

混合层：水汽混合比近似守恒

湿层：厚度约1500米

地面露点>10°C

湿层顶部露点>8°C（~850hPa)

较大的位温和相当位温直减率：

PBL的温度和露点较高

中层温度和露点较低

2）不稳定性

与对流不稳定（对流不稳定）相关。

$$\frac{\partial \theta_e}{\partial t} < 0$$

(由于整层抬升造成的条件性不稳定。逆温层被抬升时，上部比下部降温快，环境的减温率可能变为条件性不稳定)

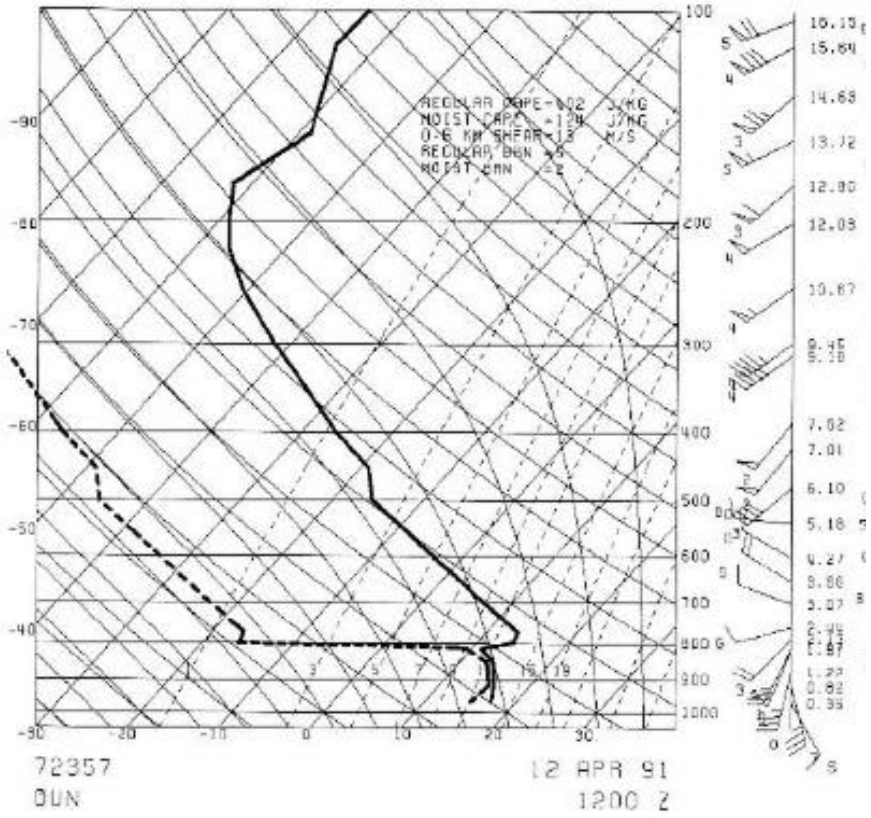

- CAPE>1500 J/kg
- TT>48 (isolated severe storm 44-46)
- LI<-3
- $|\mathrm{CIN}| \geq 100\ \mathrm{J/kg}$

3）上部干空气层预示蒸发冷却造成的强下沉气流

4）地点： 美国春季平原地区

5）气团来源：
低层湿空气来自热带海洋性气团
CAP来自热带大陆气团

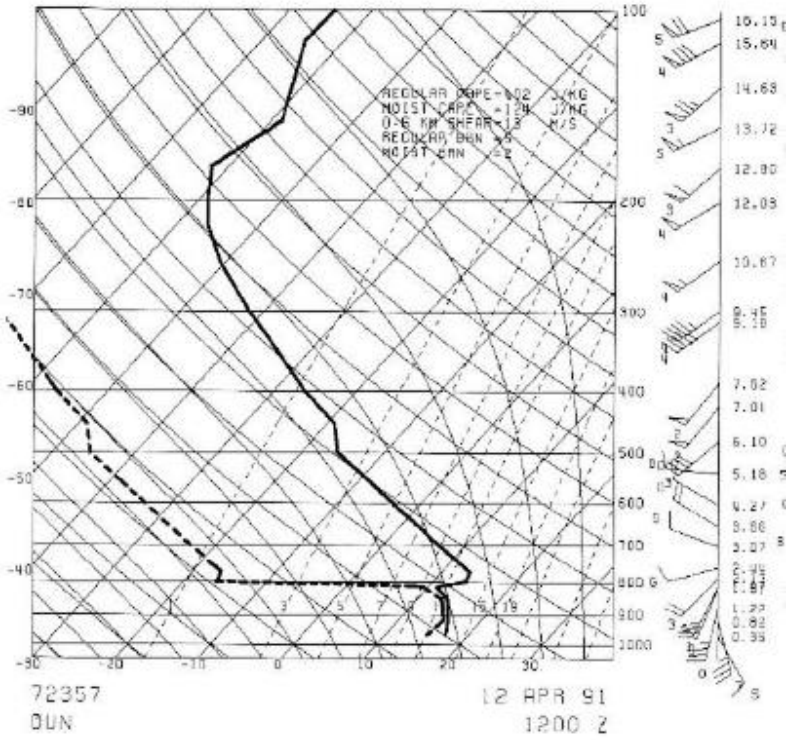

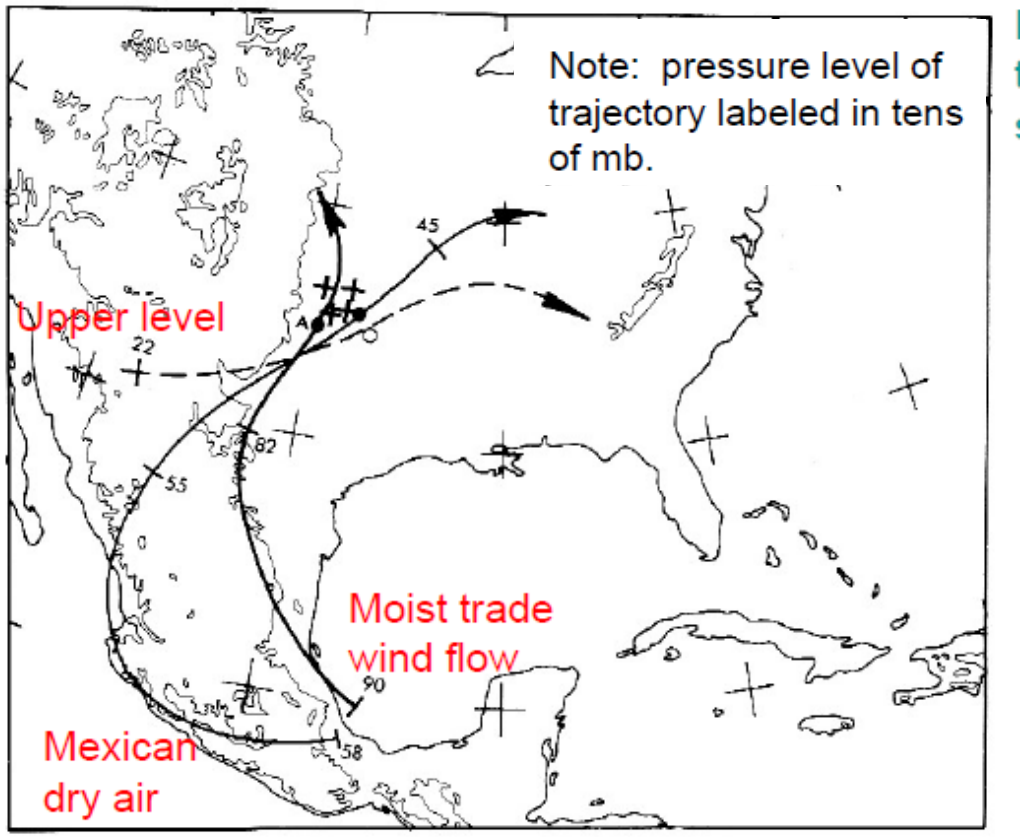

Figure 3.11. Illustration of air trajectories that produce Miller "Type I" soundings in the United States. Composite chart for May 4, 1961. Limiting trajectories for the moist, trade-wind flow (thick line; height of top of layer indicated in tens of mb) and the top of the Mexican air (thin line; height marked in tens of mb). Flow in the high troposphere, at about 220 mb (dashed line). Altus (A) and Oklahoma City (O) denoted by full circles (from Carlson and Ludlam, 1963; courtesy Toby Carlson).

Bluestein (1993)

6）垂直风切变 Veering

地面 – 850 hPa 10 m/s

地面 – 500 hPa 15 m/s

7）天气

冰雹，强风，龙卷

短时强降水，闪电

8）预报

All or nothing

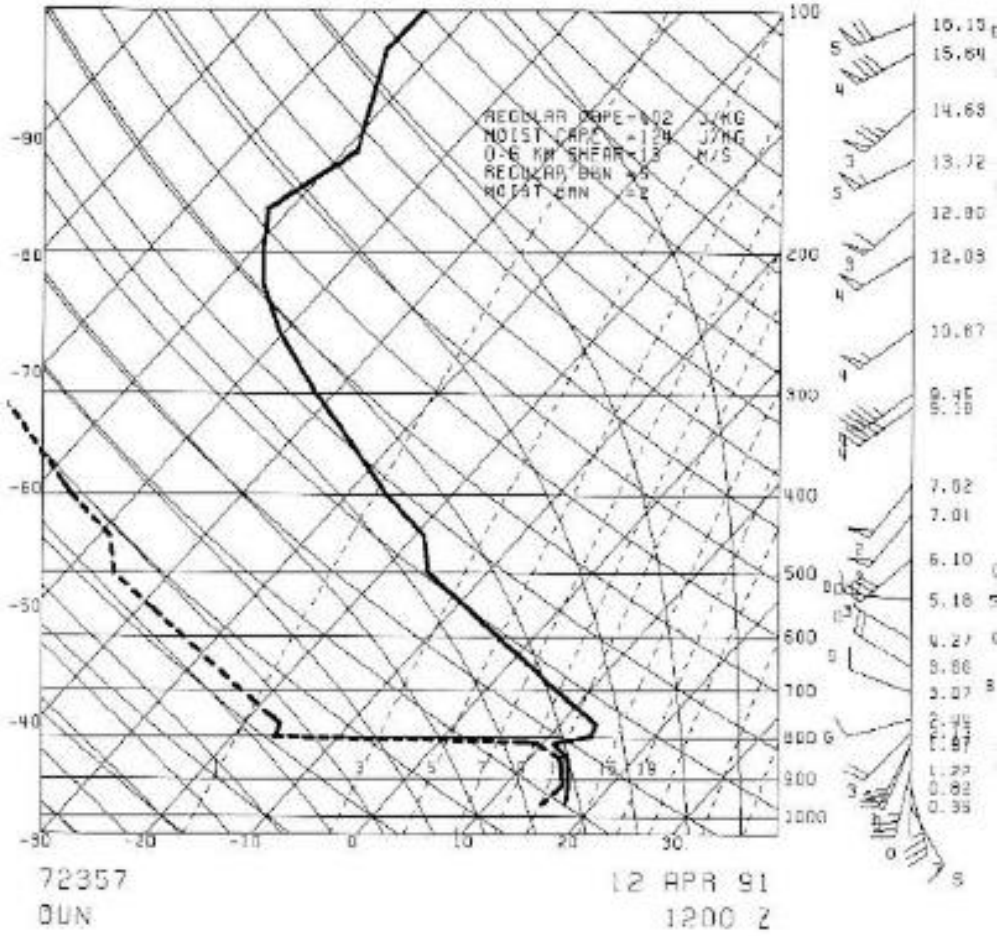

（2） 第二类Miller探空，“Tropical Sounding”

1） 特征：

- 深湿层

  RH>60-65% 约7km厚
- 一般没有Capping inversion
- 条件性不稳定 $\Gamma_m < \gamma < \Gamma_d$

  CAPE：低到中

  LI：接近于0但是是负值
- |CIN|很低或者为0
- Shear: 弱

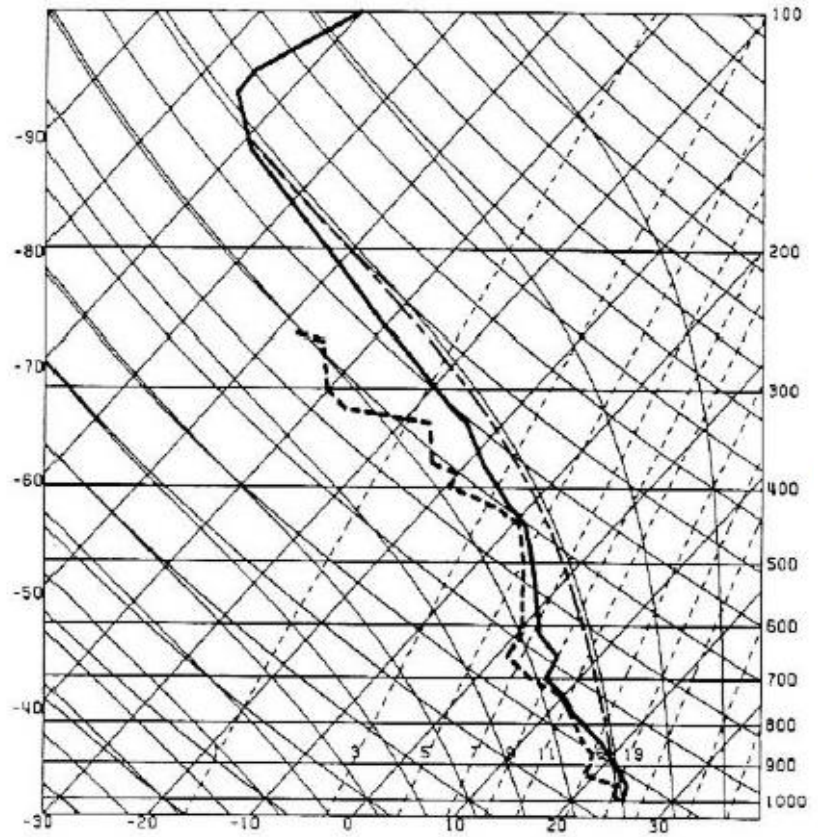

Figure 3.12 Example of a Miller "Type II" sounding in the United States. Skewed abscissa and logarithmic ordinate are temperature (°C) and pressure (mb). Temperature (solid line); dew point (dashed line); moist-adiabat along which surface air parcel ascends (dot-dashed line). For Centerville, Alabama, 0000 UTC, August 17, 1985. This sounding was associated with a tornado outbreak and the remains of Hurricane Danny (from McCaul, 1987). (Courtesy of the American Meteorological Society)

Bluestein (1993)

2）天气

大范围内出现中等强度的对流。

湿下击暴流 （ Drag， melting)

Flooding （水汽丰富）

一般不会有冰雹（high melting level)、龙卷(weak shear)

3）地点

热带地区。

美国墨西哥湾东南岸的春、夏季

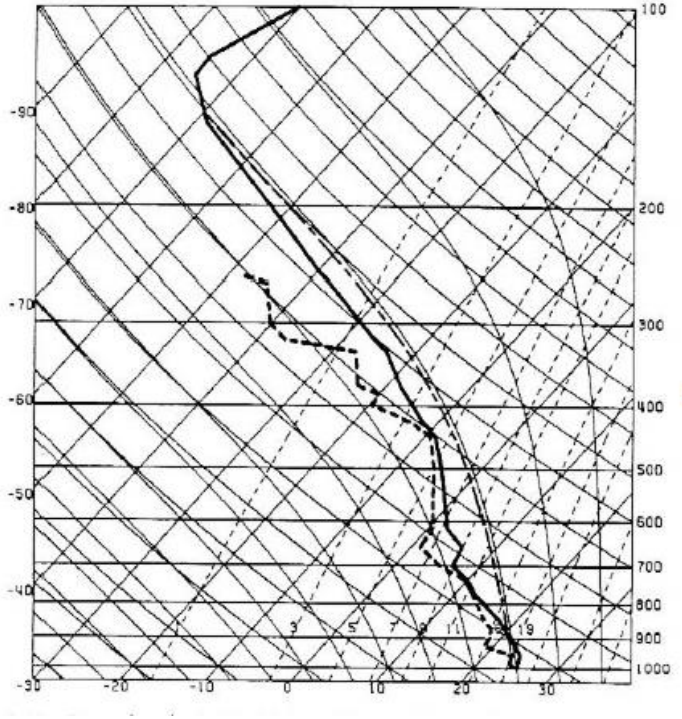

（3） 第三类Miller探空，“Cold-air sounding”

1) 特征:

- 类似于第二类热带探空，只是冷10-15 °C
- 常与高空冷涡相伴

CAPE: 低到中

- |CIN|很低或者为0
- Shear: 弱

2) 天气

有可能有冰雹 (low melting level)

3) 地点

美国高纬度的春季西海岸

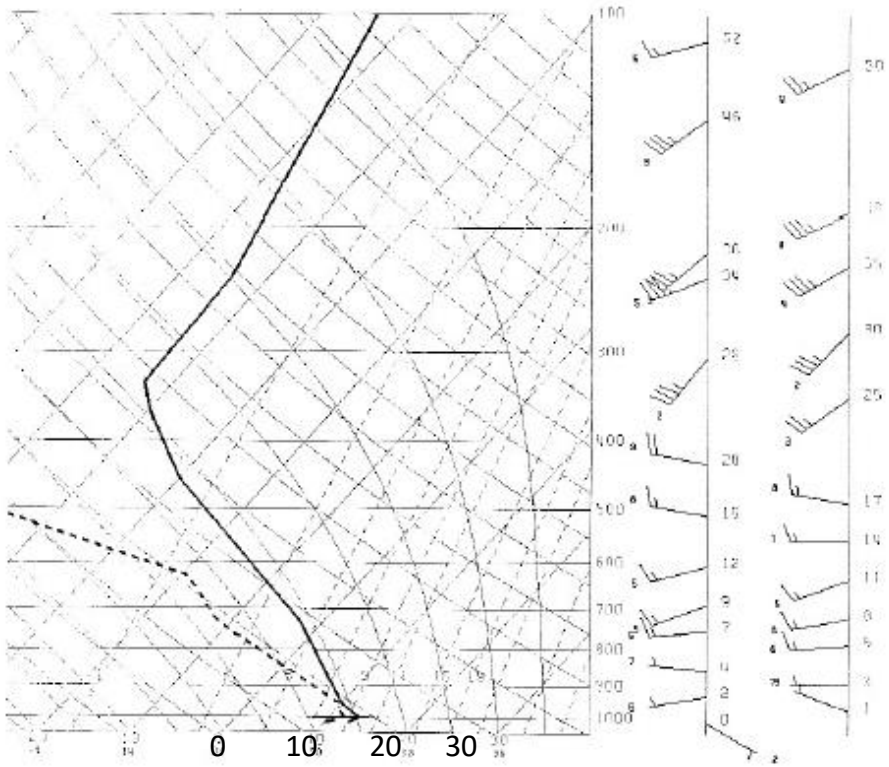

Figure 3.13 Example of a Miller "Type III" sounding in the United States. Sounding for Oakland, California, 1200 UTC, September 10, 1985. Skewed abscissa and logarithmic ordinate are temperature (°C) and pressure (mb), respectively. The plot of temperature and dew point are given by the thick solid and dashed lines, respectively. Winds plotted at the right; whole barb = 5 m s $^{-1}$; half barb = 2.5 m s $^{-1}$. A waterspout was reported over nearby San Francisco Bay near the time of this sounding. A cold upper-level low was situated over Northern California. Note the relatively cold −25°C temperature at 500 mb, and the relatively low tropopause (about 325 mb); also note the weak vertical wind shear and light land breeze at the surface from the southeast.

Bluestein (1993)

（4） 第四类Miller探空，“Inverted-V Sounding”

1) 特征:

- 探空低层类似倒V字

  低层很干

  对流层低层RH随高度增加

  较高的地面温度

  深厚的较好的PBL混合

  （露点线沿着等饱和比湿线，

  温度线沿着等位温线）

- CAPE：低
- |CIN|很低
- Shear: 无规律

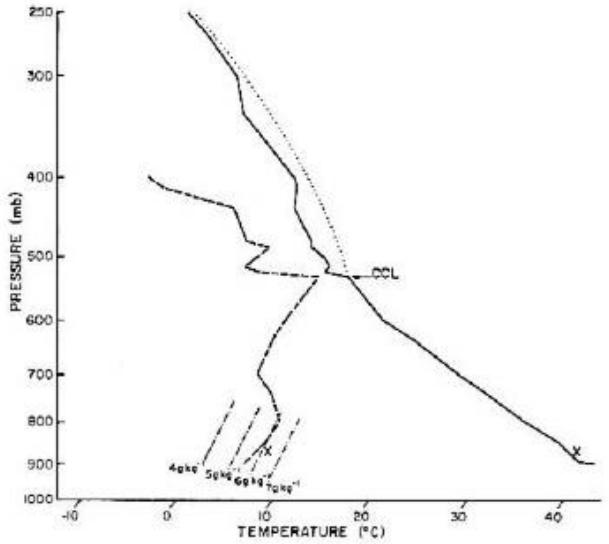

Figure 3.14 Example of a Beebe "Type IV" sounding in the United States (Desert Rock Airport, Mercury, Nevada at 0000 UTC, August 8, 1978). Skewed abscissa and logarithmic ordinate are temperature (°C) and pressure (mb). Temperature (solid line); dew point (dashed line); lines of constant saturation water-vapor mixing ratio (dash-dotted lines); moist adiabat at and above CCL (dotted line). The author observed a tornado in the Sierra Nevada region of California in an environment that was probably similar to this sounding (from Bluestein, 1979). (Courtesy of the American Meteorological Society)

Bluestein (1993)

2）天气

高架对流 （550-500 hPa)

强风，干下击暴流

3）地点

美：高海拔平原地区，西部高原， 位于干线的后面，干的热带大陆气团在极地海洋气团之下。

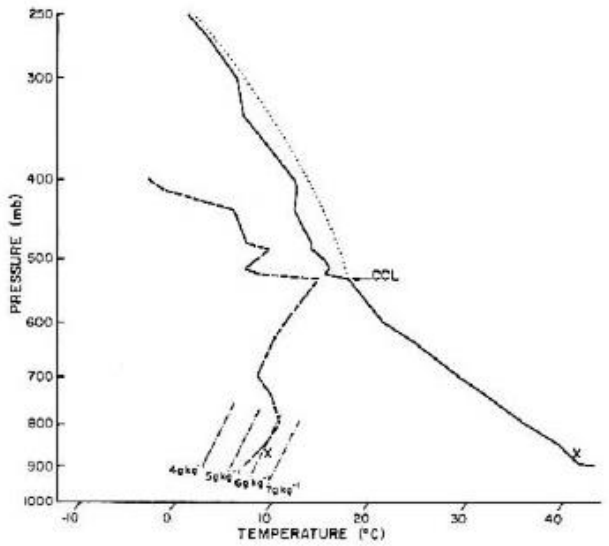

Figure 3.14 Example of a Beebe "Type IV" sounding in the United States (Desert Rock Airport, Mercury, Nevada at 0000 UTC, August 8, 1978). Skewed abscissa and logarithmic ordinate are temperature (°C) and pressure (mb). Temperature (solid line); dew point (dashed line); lines of constant saturation water-vapor mixing ratio (dash-dotted lines); moist adiabat at and above CCL (dotted line). The author observed a tornado in the Sierra Nevada region of California in an environment that was probably similar to this sounding (from Bluestein, 1979). (Courtesy of the American Meteorological Society)

Bluestein (1993)

典型探空

(1) 第一类Miller探空，“Loaded Gun”

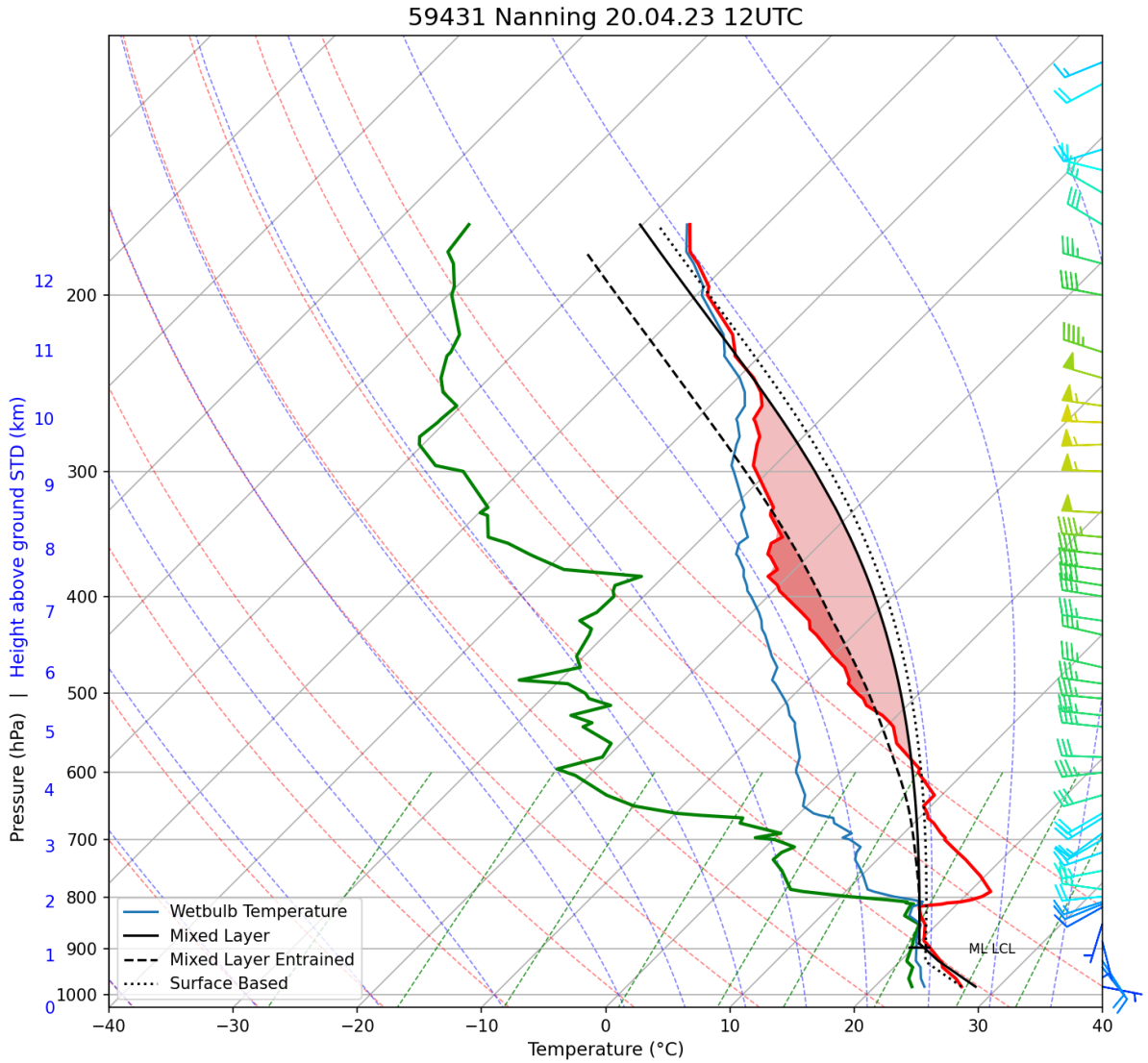

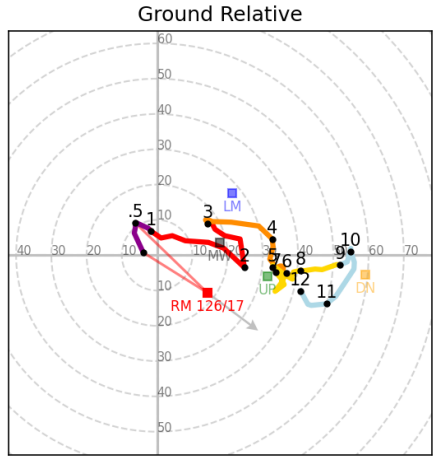

0°C AMSL (m):	5307
Total Totals	47.5
PWAT (mm)	42
DCAPE (J/kg)	212
Mixed Layer Parcel	
LCL AGL (m)	876
LFC AGL (m)	4512
Lifted Index	-3.5
CAPE | CIN (J/kg)	1048 | -253
ECAPE | ECIN (J/kg)	220 | -320
Surface Based Parcel	
LCL AGL (m)	514
LFC AGL (m)	4152
Lifted Index	-4.3
CAPE | CIN (J/kg)	1355 | -214
Wind and Hodograph	
RM Dir (°)	126
RM Spd (kn|km/h)	17 | 33
Shear 0-1 km (kn)	6
Shear 0-6 km (kn):	39
SRH 0-1 km (m^2/s^2)	49
SRH 0-3 km (m^2/s^2)	79
Eff. Inflow HGT (b|t)(m):	1 | 514
RM Inflow SPD (b|t)(kn):	21 | 28
Composite Parameters	
SigTor:	0.6
SupComp:	2.1
SHIP Index	0.33

Lat: 22.47 Lon: 108.33
station elevation: 152 m

典型探空

（2） 第二类Miller探空，“Tropical Sounding”

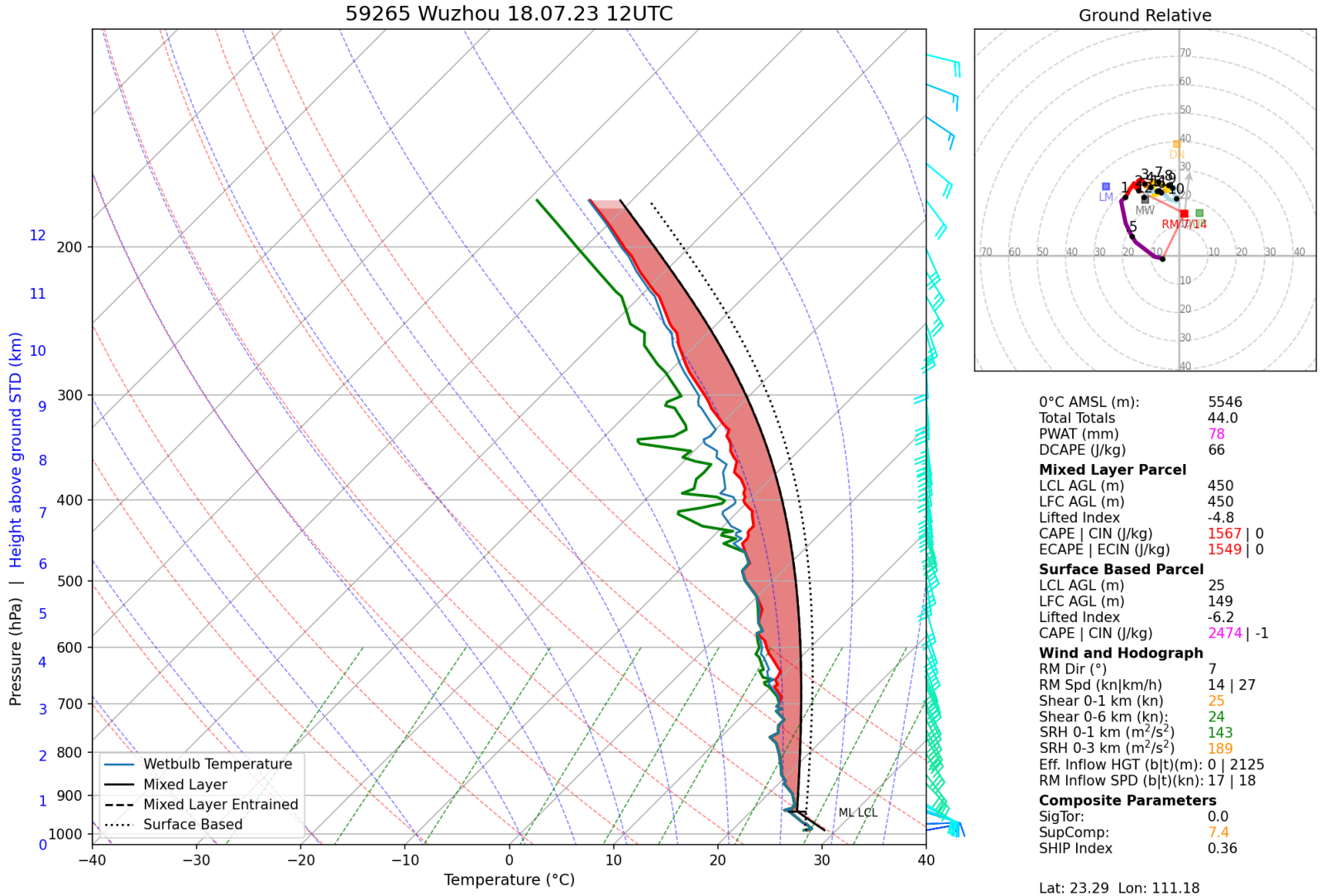

0°C AMSL (m):	5546
Total Totals	44.0
PWAT (mm)	78
DCAPE (J/kg)	66
Mixed Layer Parcel	
LCL AGL (m)	450
LFC AGL (m)	450
Lifted Index	-4.8
CAPE | CIN (J/kg)	1567 | 0
ECAPE | ECIN (J/kg)	1549 | 0
Surface Based Parcel	
LCL AGL (m)	25
LFC AGL (m)	149
Lifted Index	-6.2
CAPE | CIN (J/kg)	2474 | -1
Wind and Hodograph	
RM Dir (°)	7
RM Spd (kn|km/h)	14 | 27
Shear 0-1 km (kn)	25
Shear 0-6 km (kn):	24
SRH 0-1 km (m^2/s^2)	143
SRH 0-3 km (m^2/s^2)	189
Eff. Inflow HGT (b|t)(m):	0 | 2125
RM Inflow SPD (b|t)(kn):	17 | 18
Composite Parameters	
SigTor:	0.0
SupComp:	7.4
SHIP Index	0.36

Lat: 23.29 Lon: 111.18
station elevation: 120 m

典型探空

（3） 第三类Miller探空，“Cold-air sounding”

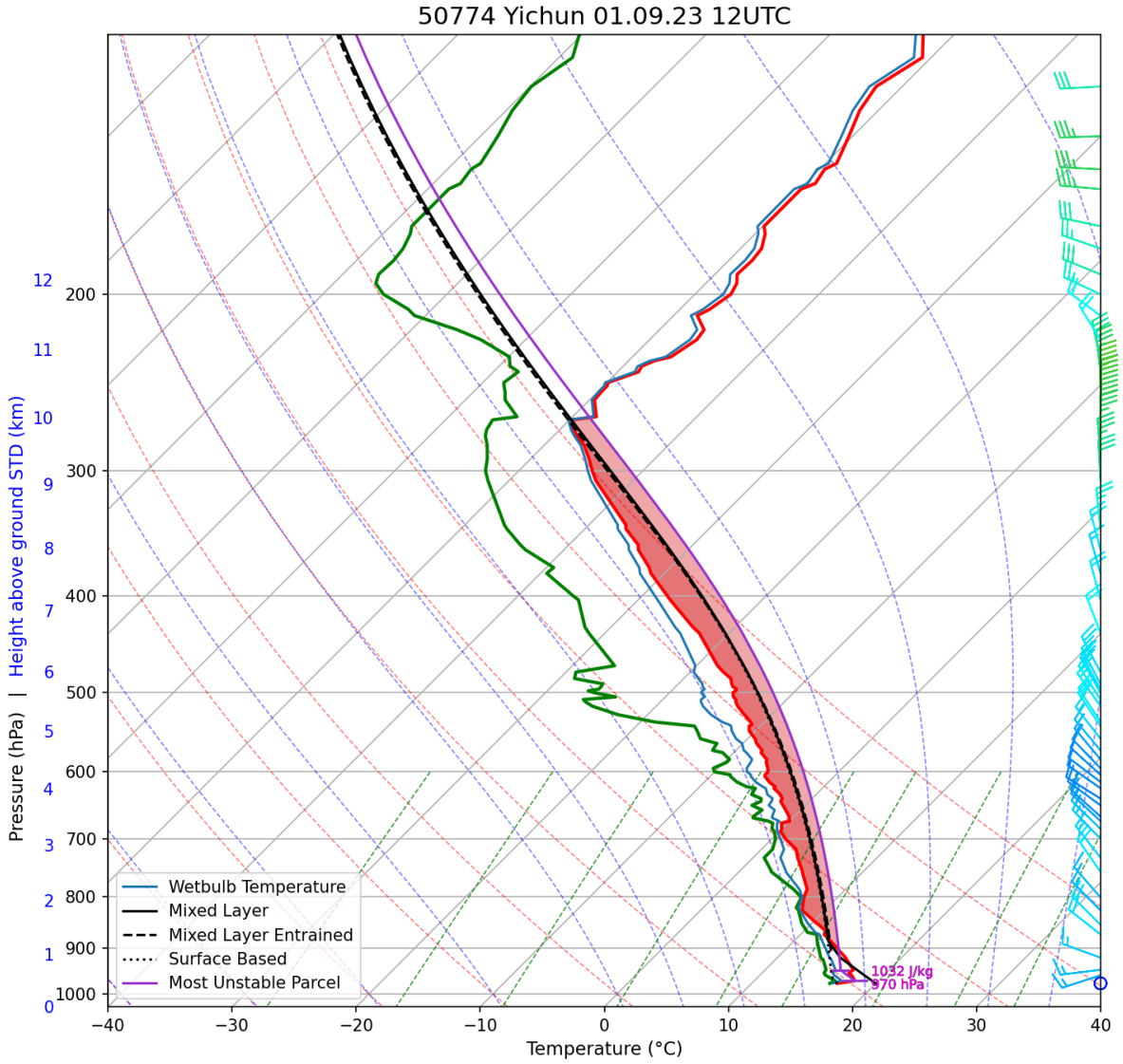

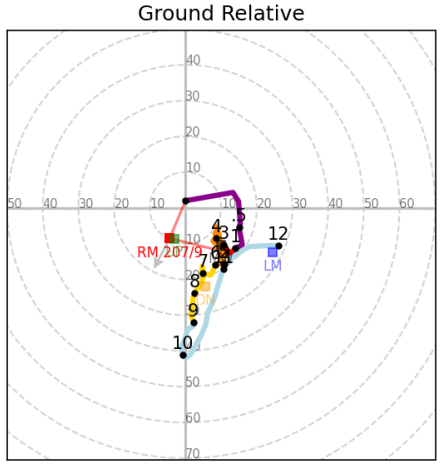

0°C AMSL (m):	3215
Total Totals	49.4
PWAT (mm)	32
DCAPE (J/kg)	82
Mixed Layer Parcel	
LCL AGL (m)	823
LFC AGL (m)	994
Lifted Index	-2.0
CAPE | CIN (J/kg)	600 | -2
ECAPE | ECIN (J/kg)	594 | -5
Surface Based Parcel	
LCL AGL (m)	56
LFC AGL (m)	994
Lifted Index	-1.9
CAPE | CIN (J/kg)	572 | -34
Wind and Hodograph	
RM Dir (°)	207
RM Spd (kn|km/h)	9 | 17
Shear 0-1 km (kn)	19
Shear 0-6 km (kn):	21
SRH 0-1 km (m^2/s^2)	133
SRH 0-3 km (m^2/s^2)	128
Eff. Inflow HGT (b|t)(m):	1 | 1145
RM Inflow SPD (b|t)(kn):	11 | 17
Composite Parameters	
SigTor:	0.0
SupComp:	1.4
SHIP Index	0.09

Lat: 47.43 Lon: 128.5
station elevation: 265 m

典型探空

（4） 第四类Miller探空，“Inverted-V Sounding”

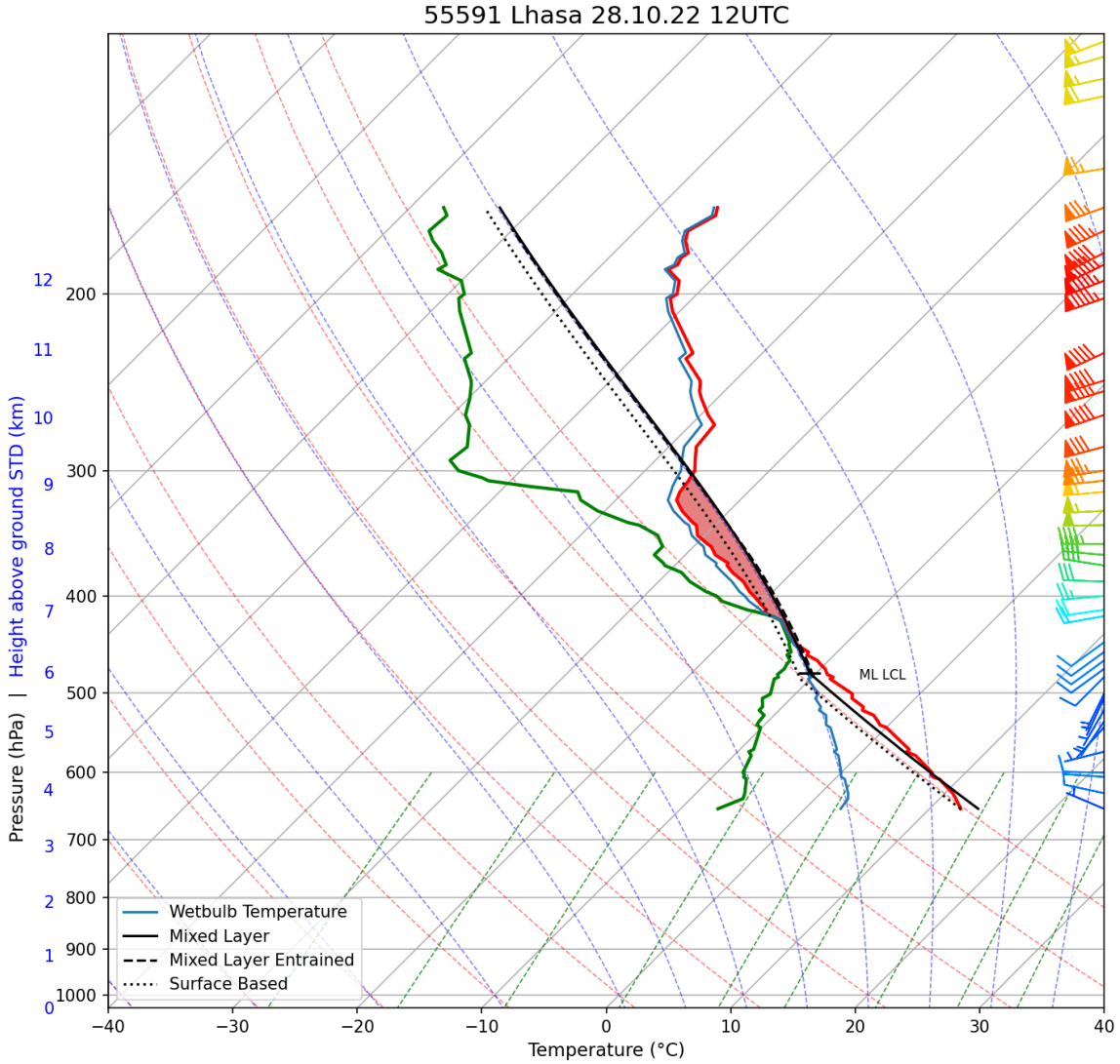

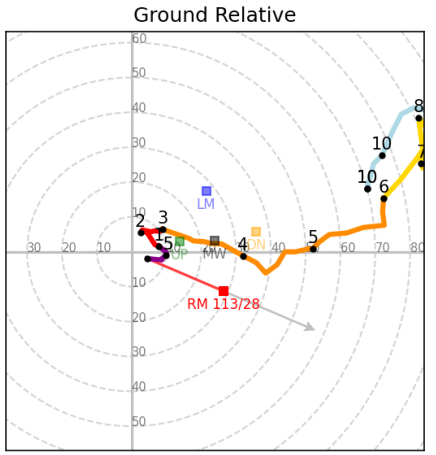

0°C AMSL (m):	5165
Total Totals	nan
PWAT (mm)	9
DCAPE (J/kg)	763
Mixed Layer Parcel	
LCL AGL (m)	2470
LFC AGL (m)	2971
Lifted Index	1.5
CAPE | CIN (J/kg)	198 | -55
ECAPE | ECIN (J/kg)	207 | -73
Surface Based Parcel	
LCL AGL (m)	2402
LFC AGL (m)	3471
Lifted Index	2.8
CAPE | CIN (J/kg)	88 | -212
Wind and Hodograph	
RM Dir (°)	113
RM Spd (kn|km/h)	28 | 53
Shear 0-1 km (kn)	4
Shear 0-6 km (kn):	77
SRH 0-1 km (m^2/s^2)	22
SRH 0-3 km (m^2/s^2)	56
Eff. Inflow HGT (b|t)(m):	- | -
RM Inflow SPD (b|t)(kn):	- | -
Composite Parameters	
SigTor:	0.0
SupComp:	0.2
SHIP Index	0.01

Lat: 29.4 Lon: 91.08
station elevation: 3650 m

Organized convective system的触发环境

General Features of Squall Lines in East China

ZHIYONG MENG, DACHUN YAN, AND YUNJI ZHANG

Laboratory for Climate and Ocean–Atmosphere Studies, Department of Atmospheric and Oceanic Sciences, School of Physics, Peking University, Beijing, China

Monthly variation

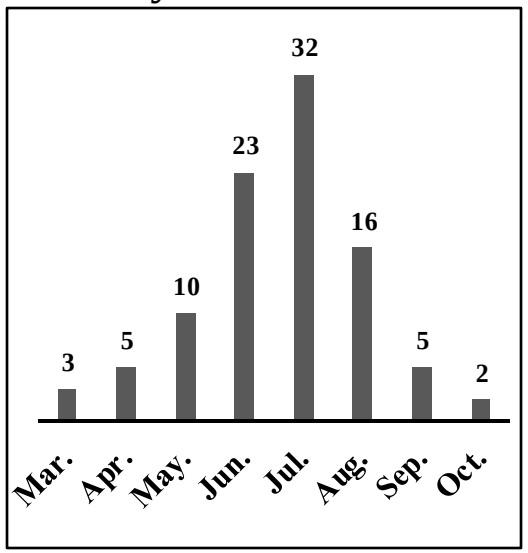

Formation frequency of squall line

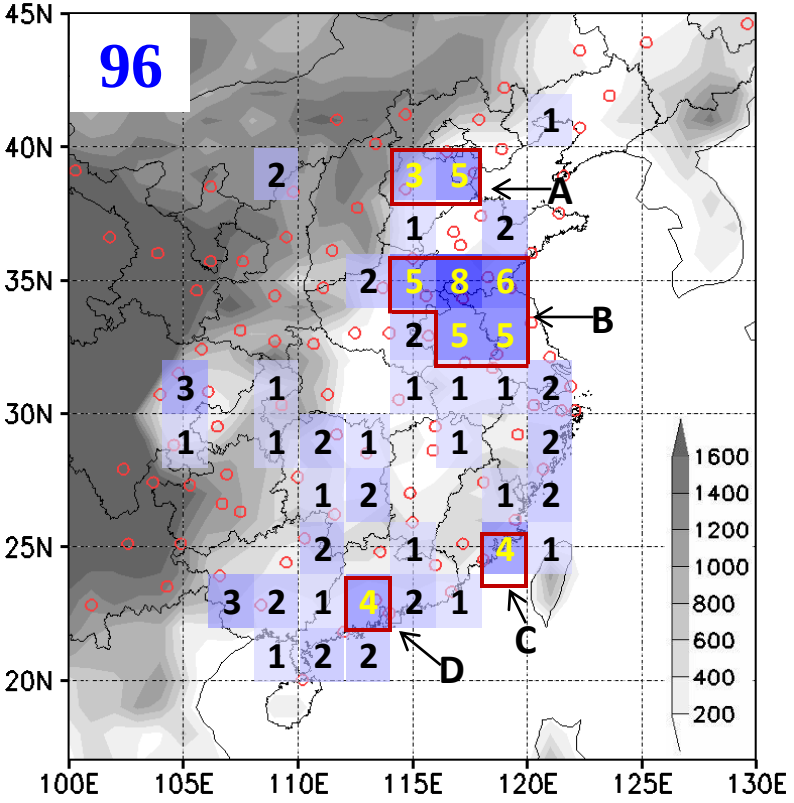

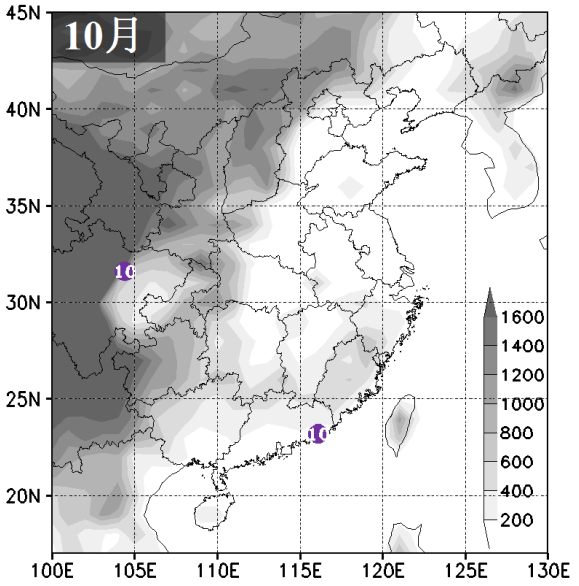

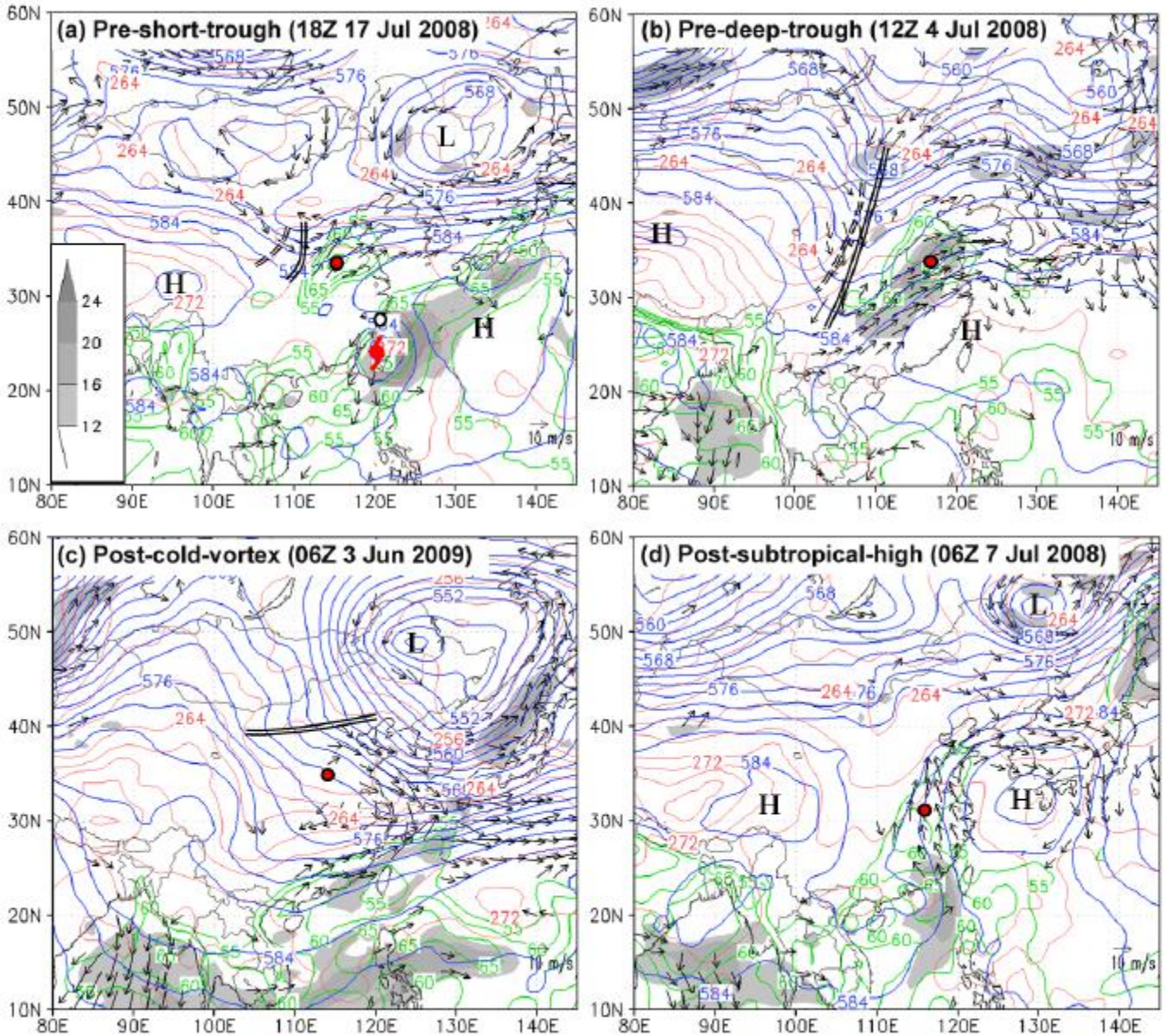

FIG. 12. Examples of various environmental flow patterns at (a) 1800 UTC 17 Jul 2008 and (b) 0000 UTC 21 Aug 2008 for pre-short-trough cases, (c) 1200 UTC 4 Jul 2008 and (d) 0000 UTC 23 Jul 2008 for pre-long-trough cases, (e) 0600 UTC 3 Jun 2009 and (f) 0000 UTC 14 Jun 2009 for cold-vortex cases, (g) 0000 UTC 29 Jun 2008 and (h) 0600 UTC 7 Jul 2008 for subtropical-high cases, and (i) 0000 UTC 16 May 2008 for posttrough cases. Plotted are geopotential height [blue contours, 10 geopotential meters (gpm)], temperature (dashed red contours, K) at 500 hPa, column-integrated PW greater than 55 kg m^{-2} (green contours, kg m^{-2}), vertical shear vector between 700 and 1000 hPa with the magnitude larger than 8 m s^{-1} [the representative wind vector is given in the bottom-right corner of (a)], and wind speed larger than 9 m s^{-1} at 850 hPa (shaded, every 3 m s^{-1}). The double solid brown lines denote the trough at 500 hPa. The red solid contour and the double solid black lines in (i), respectively, denote the geopotential height (10 gpm) and the trough at 850 hPa. The places where the convection of the squall line was initiated are marked by red dots. The white dots indicate the areas that also have a possibility of squall-line formation near a TC. Here, H and L denote the high and low pressure centers at 500 hPa, respectively. The TC centers are given by the red typhoon marks in (a) and (b).

14

11

9

5

台风前部飑线

On the Squall Lines Preceding Landfalling Tropical Cyclones in China

ZHIYONG MENG AND YUNJI ZHANG

Laboratory for Climate and Ocean–Atmosphere Studies, Department of Atmospheric and Oceanic Sciences, School of Physics, Peking University, Beijing, China

Representative mosaics, isochrones with formation and dissipation times

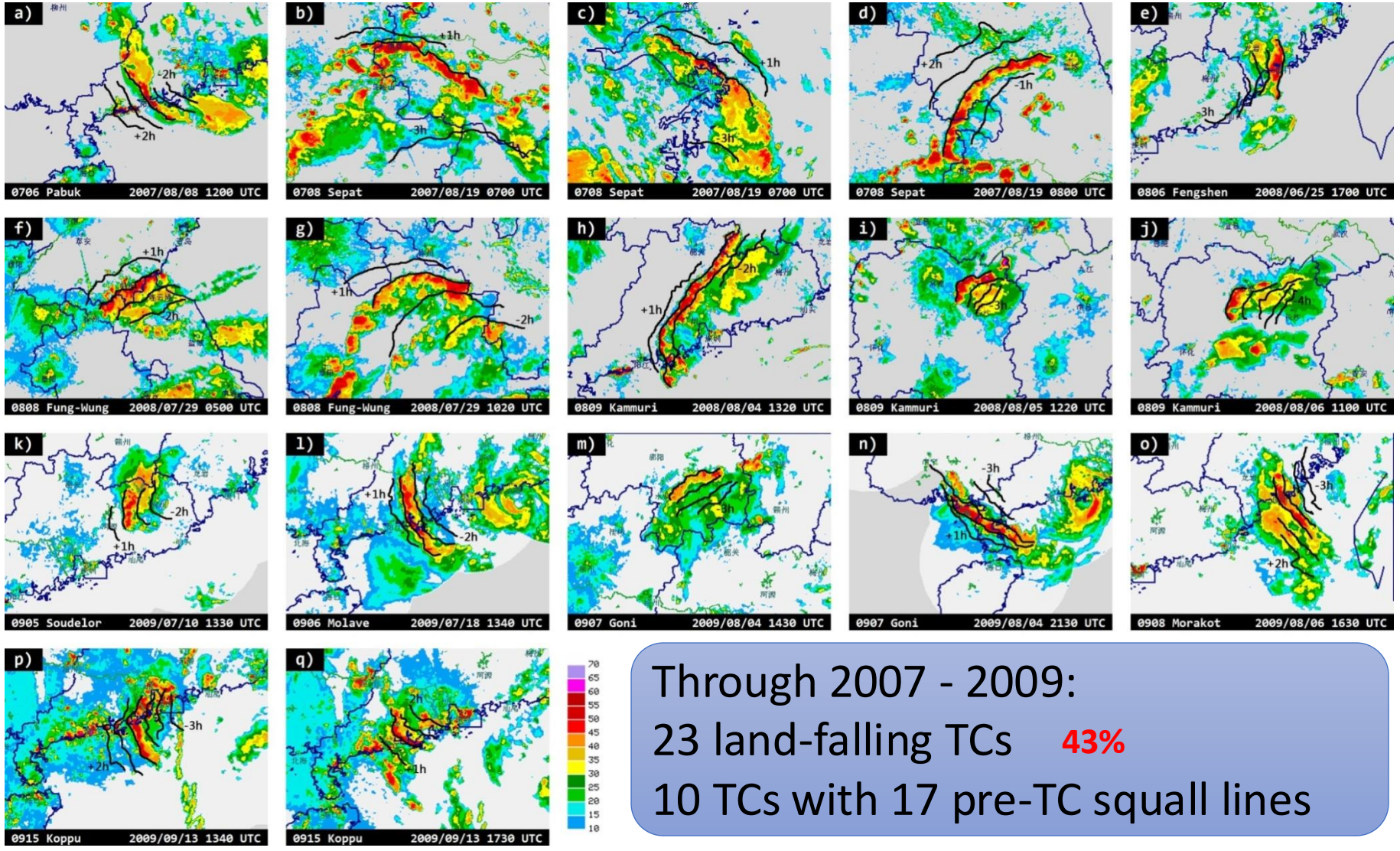

Through 2007 - 2009:
23 land-falling TCs **43%**
10 TCs with 17 pre-TC squall lines

台风前部飑线的组合背景

$$F = \frac{D}{Dt}\left|\nabla_p \theta\right|$$

FIG. 8. Composite analysis of 925-hPa frontogenesis [10^2 K km^{-1} (3 h)$^{-1}$; shaded], 850-hPa geopotential height (black contour every 10 gpm), and wind vector (full barb =10 m s^{-1}) as well as column-integrated precipitable water (red contour every 5 kg m^{-2}) for the 9 cases that have a westward motion component during 2007–09 at (a) −12, (b) −6, (c) 0, and (d) 6 h relative to the formation time T of pre-TC squall line. The solid square denotes the median of the formation locations of the 10 pre-TC squall lines at time T. The red TC mark denotes the TC center. (e),(f) As in (a)–(d), but for the TCs that are not associated pre-TC squall lines at 18 and 6 h before landfall.

700 hPa H , 925 hPa Frontogenesis, PW

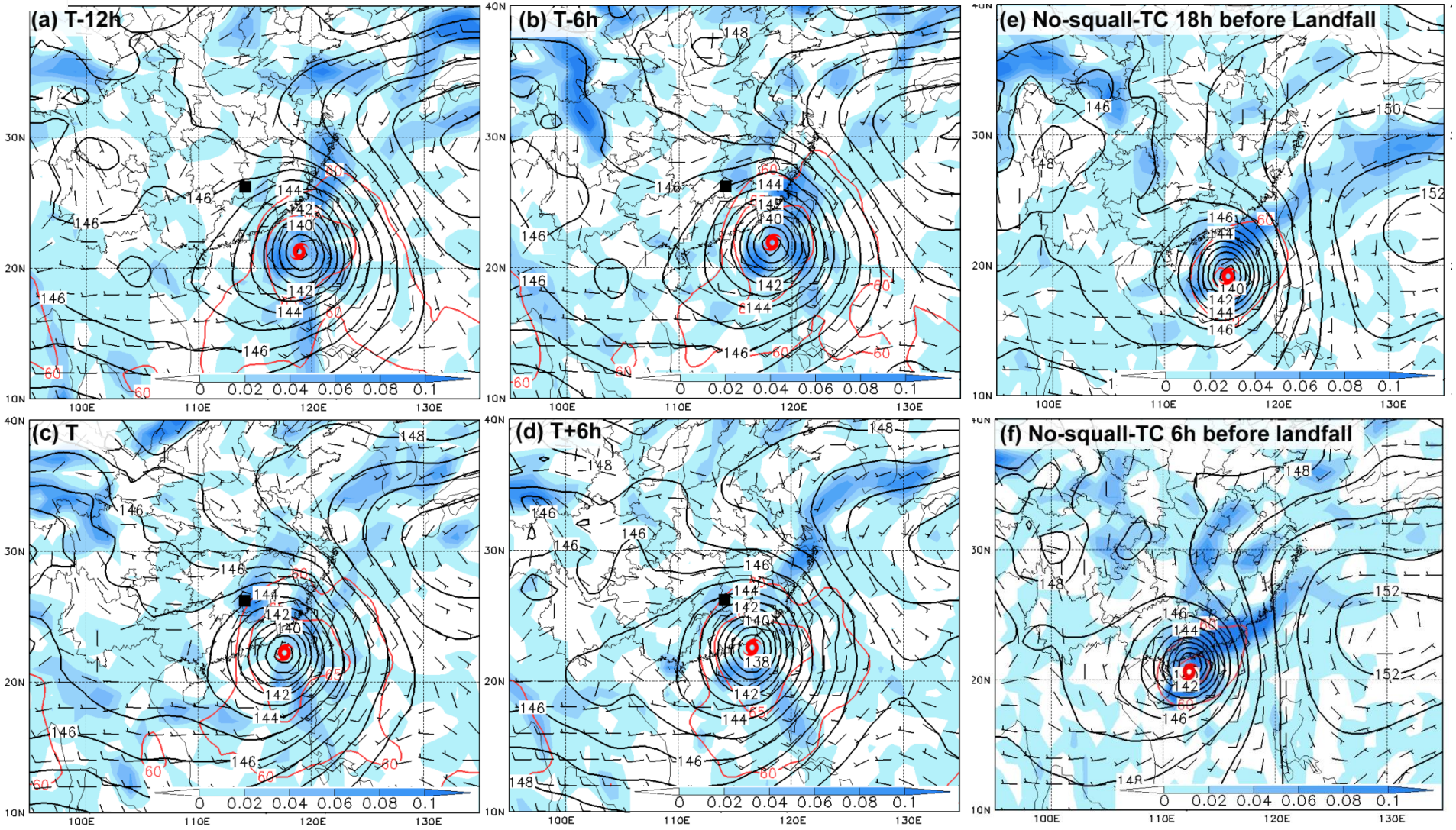

台风前部飑线的组合背景

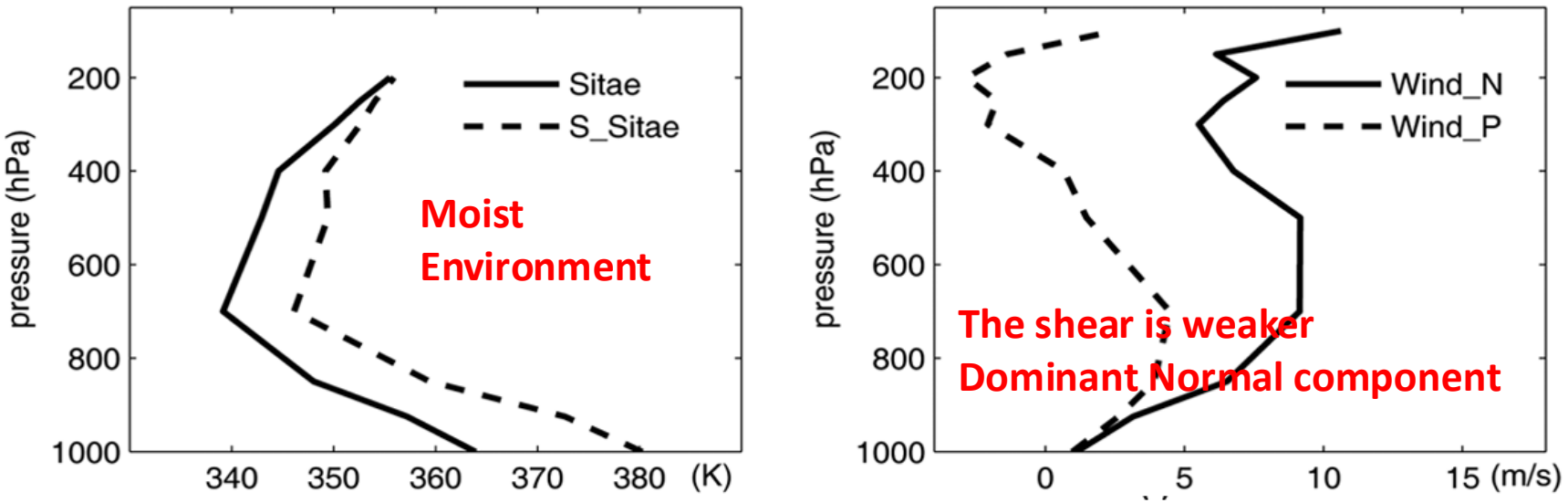

Table 2. Comparison between averages of derived properties of the environmental soundings in front of squall lines in different studies

Averages of derived properties	CAPE ($J\ kg^{-1}$)	CIN ($J\ kg^{-1}$)	LI (K)	LCL (hPa)	PW (cm)
Pre-TC squall lines	1548	67	-3.6	899	6.1
Bluestein & Jain (1985)	2260	33			2.8
Parker &Johnson (2000)	1605		-5.4	831	3.4
Wyss & Emanuel (1988)	1208	76			

Kammuri (2008)

50mm Rain, 18m/s wind gust

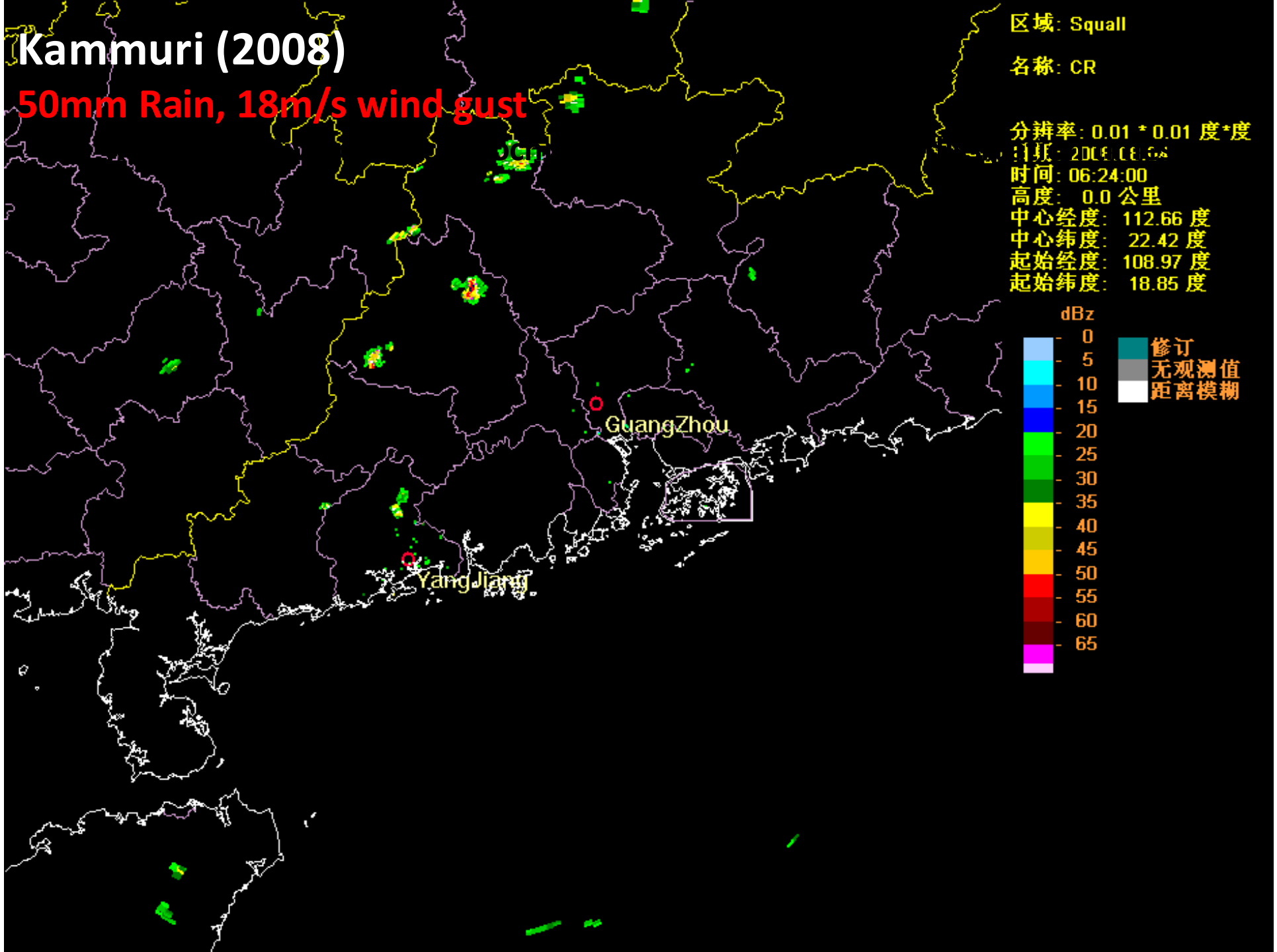

Environment: Instability & Moisture

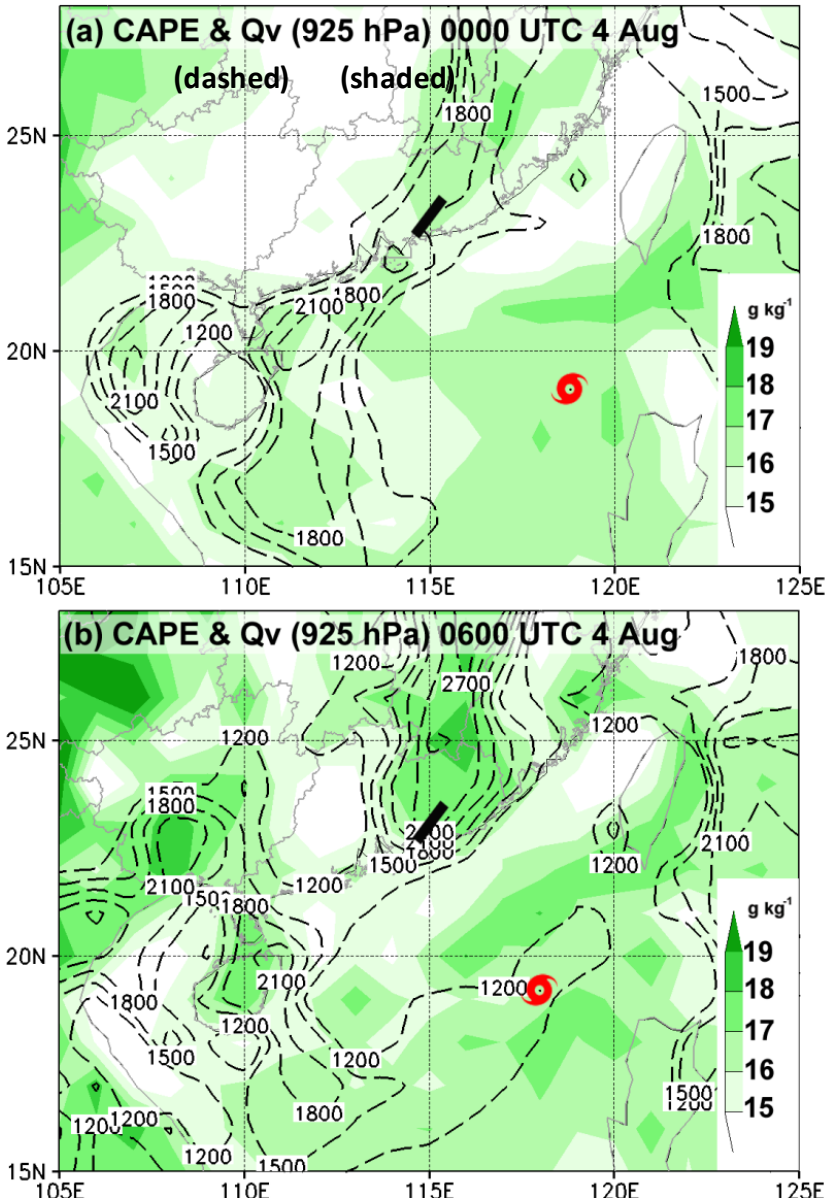

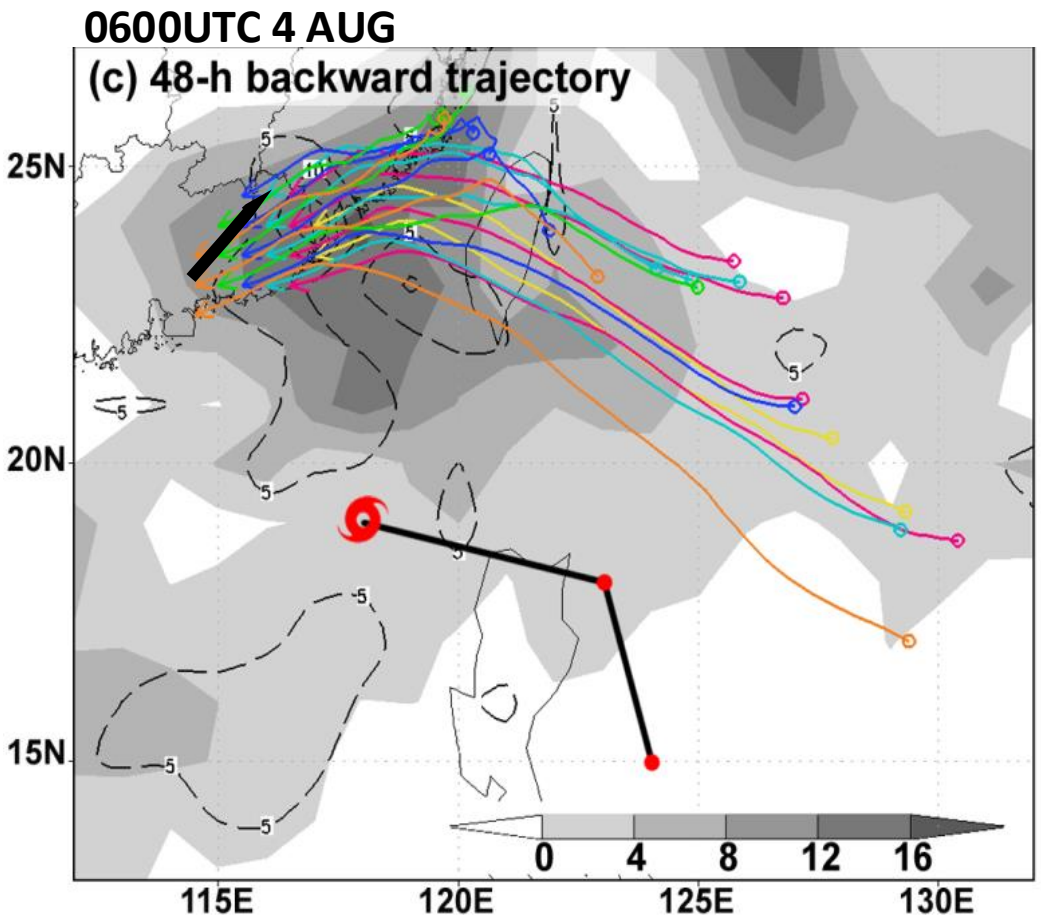

FIG. 14. Water vapor mixing ratio at 925 hPa (shaded; g kg^{-1}) and CAPE (contour; J kg^{-1}) at (a) 0000 UTC 4 Aug 2008 and (b) 0600 UTC 4 Aug 2008. The short heavy line in (a) and (b) stands for the orientation of linear growth of initial convection. The red typhoon mark denotes the center of Kammuri. (c) Also plotted are twenty 48-h backward trajectories from the area where the convection was initiated at 3-km altitude at 0600 UTC 4 Aug back to 0600 UTC 2 Aug 2008 (denoted by small circles). Different colors of the trajectories denote different longitudinal locations. The dashed lines represent the increase of relative humidity (every 5%) during the two days. The shaded area denotes the increase of precipitable water (every 4 kg m^{-2}).

Vertical motion: Synoptic forcing

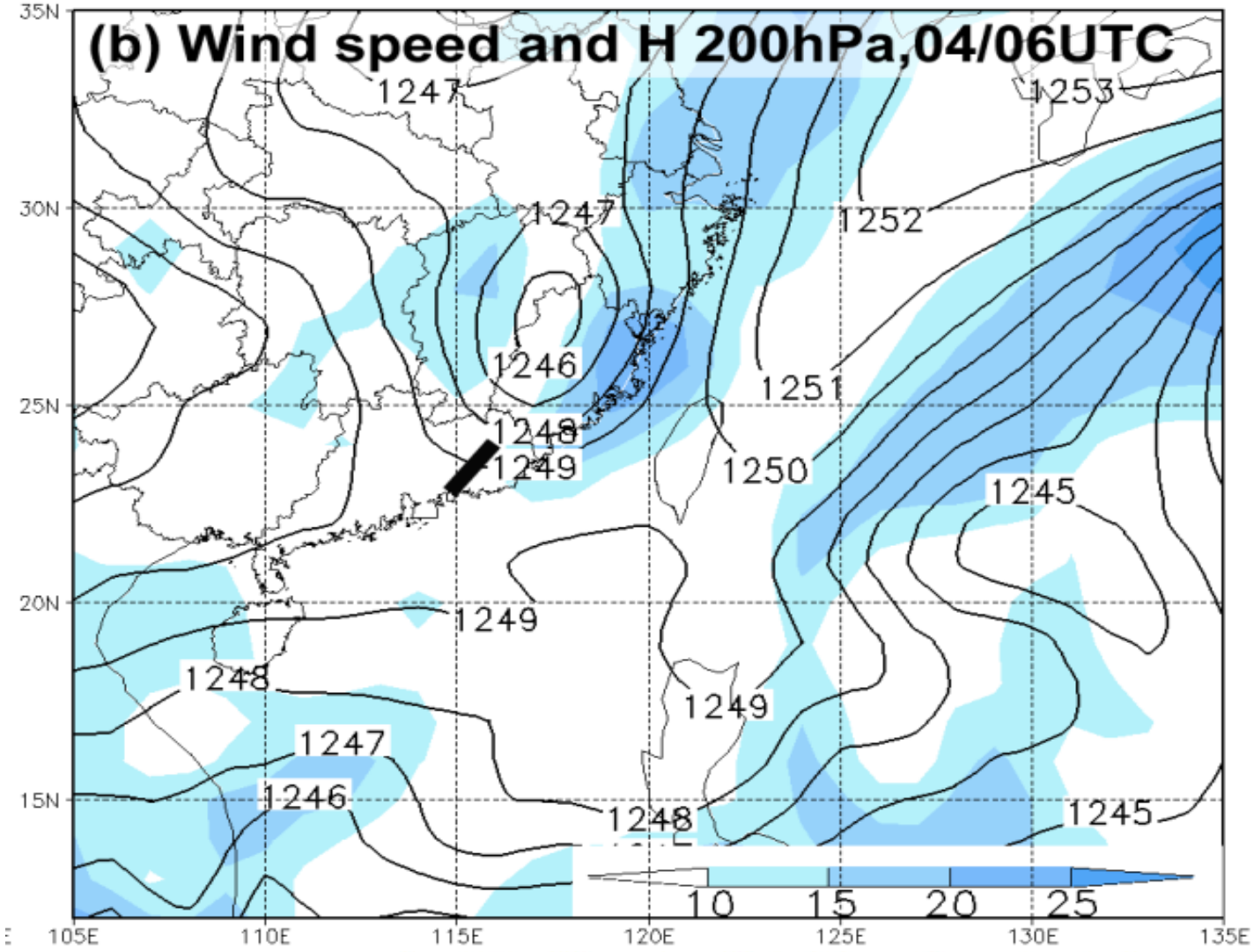

FIG. 12. 200-hPa wind speed (shaded according to the color bar in m s^{-1}) and geopotential height (solid contour every 10 gpm) at (a) 0000 and (b) 0600 UTC 4 Aug 2008. (c),(d) The dynamic tropopause (DT) potential temperature (shaded according to the color bar in K) and wind (full barb = 10 m s^{-1}) at 0000 and 0600 UTC 4 Aug 2008. The heavy short line denotes where the convection was initiated.

Vertical motion: Mesoscale forcing

Surface streamline and convergence (shaded)

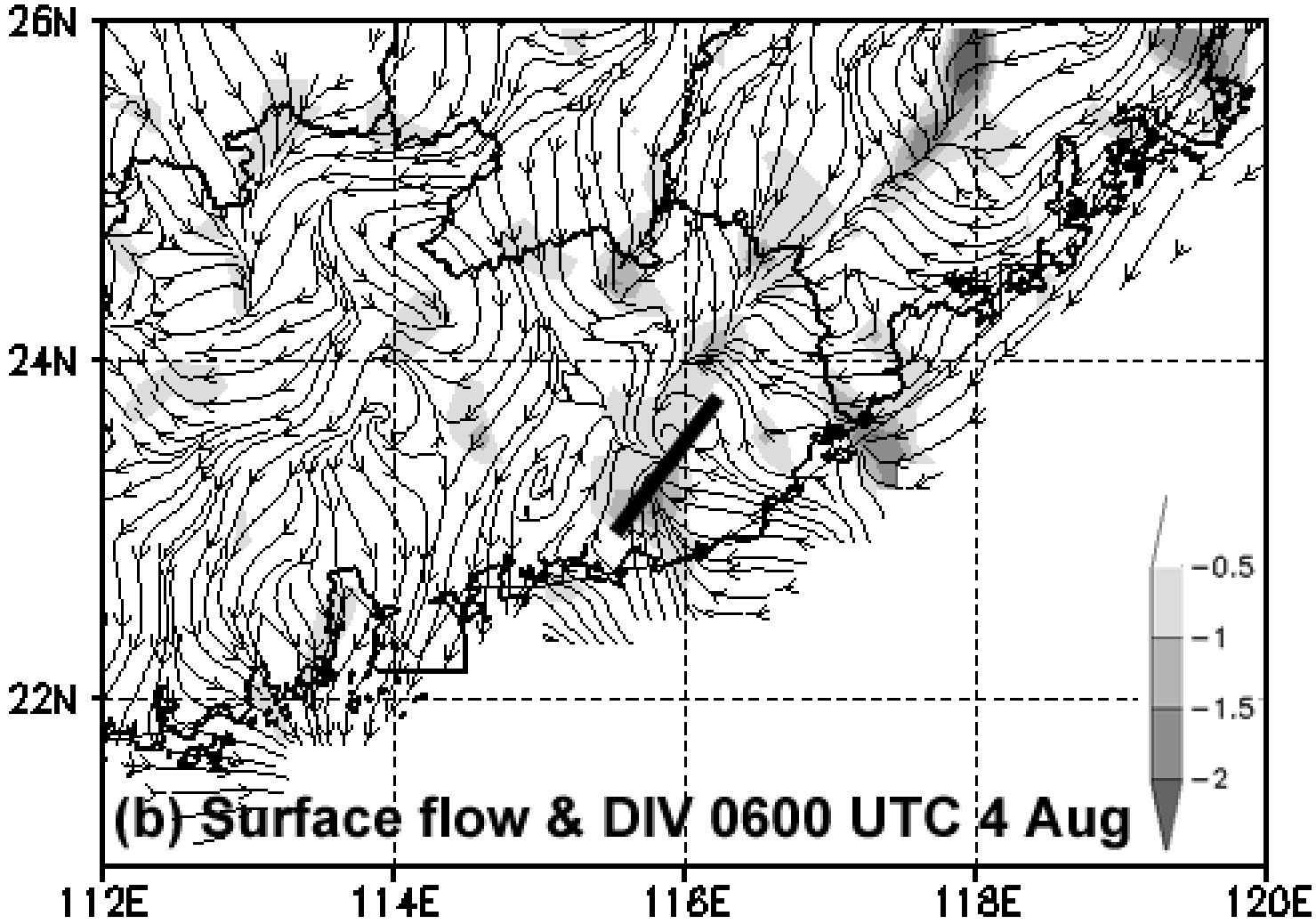

FIG. 9. Surface flow and convergence (shaded; 10^{-4} s^{-1}) at (a) 0400 and (b) 0600 UTC 4 Aug 2008. The short heavy line represents the orientation of linear growth of initial convection.

Ordinary cell convective storm

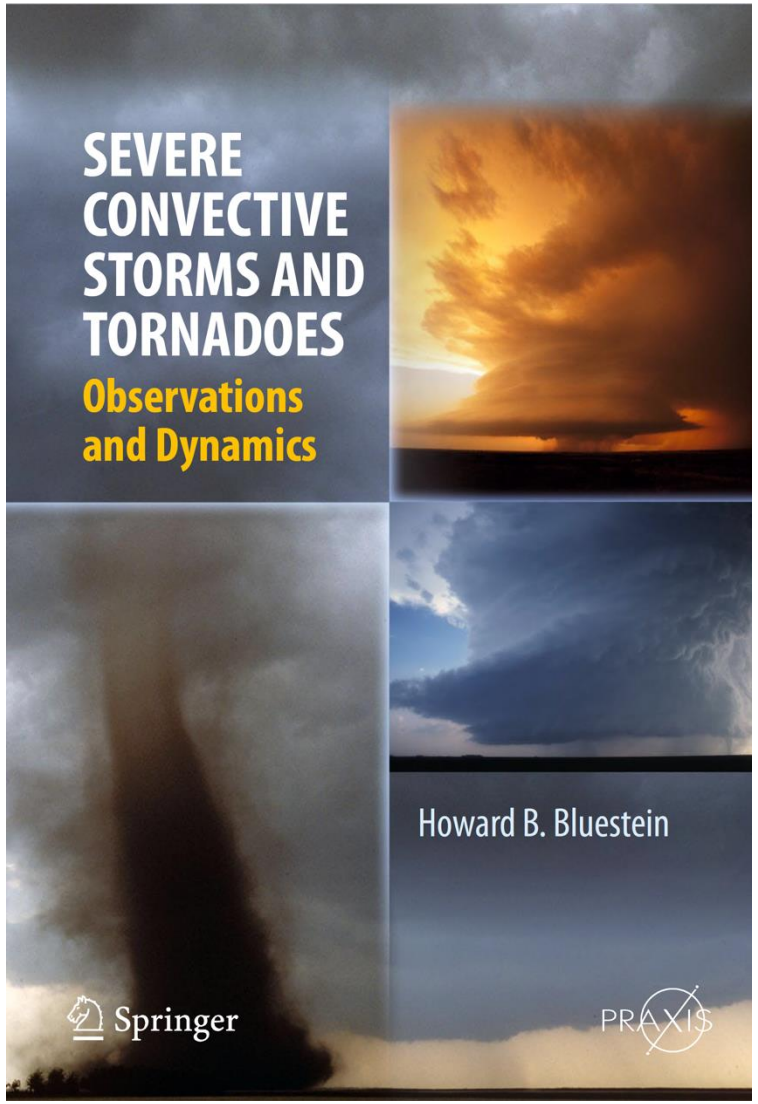

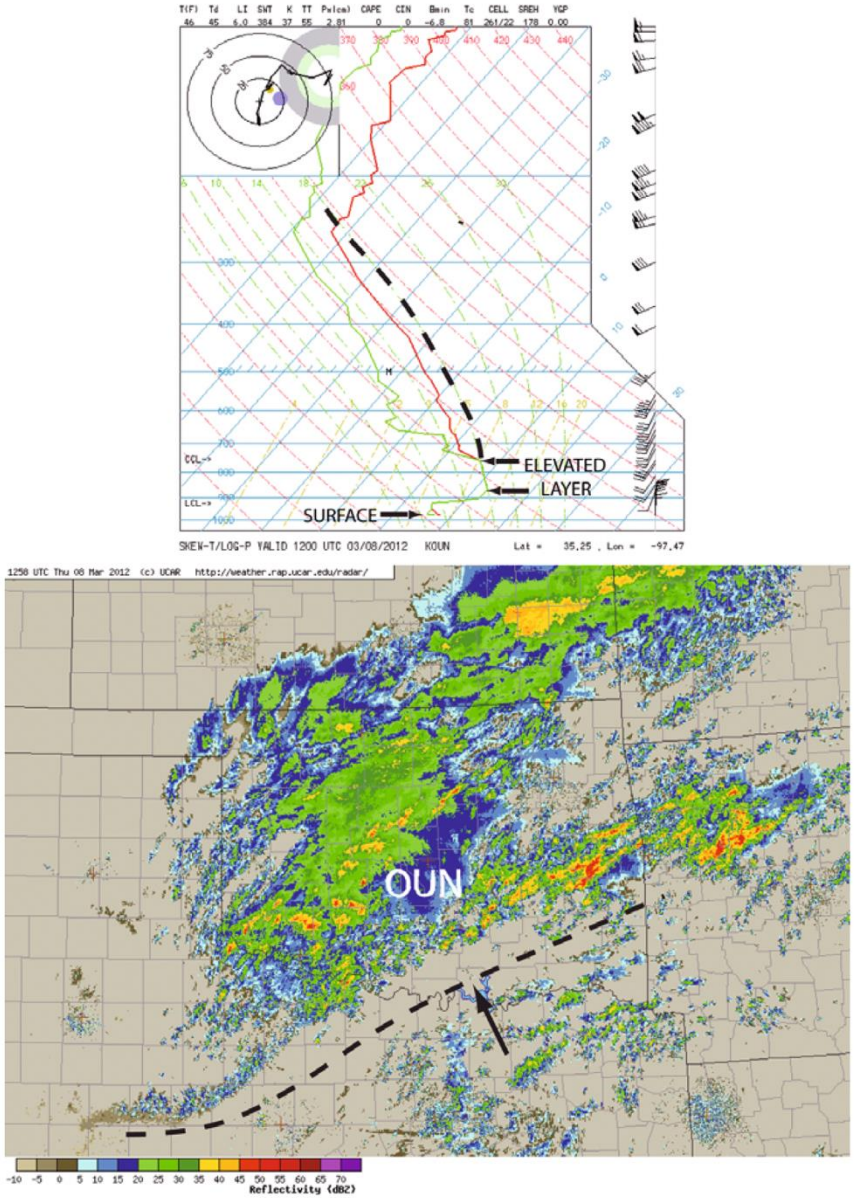

Figure 3.2a. Elevated convection. (Top) Sounding at Norman, OK (OUN) at 12:00 UTC on March 8, 2012; elevated thunderstorms as depicted by WSR-88D composite radar reflectivity in dBZ (bottom) occurring north of a cold front (dashed line at the bottom) as air flowing from the southeast (arrow in the bottom panel) rises over the frontal zone (stable layer between 920 and 870 hPa. In the top panel the elevated LCL is indicated as a saturated layer between 880 and 750 hPa. Surface parcels lifted will not attain an LCL. Above the elevated LCL, air parcels follow the moist adiabat (dashed line), where CAPE is realized.

Figure 3.2b. (Top) Altocumulus castellanus over Norman, OK on September 28, 1977 and (bottom) July 26, 1978. The bases of the clouds are flat and above the boundary layer. The clouds are also aligned in streets, possibly in response to lifting by bores (photographs by the author).

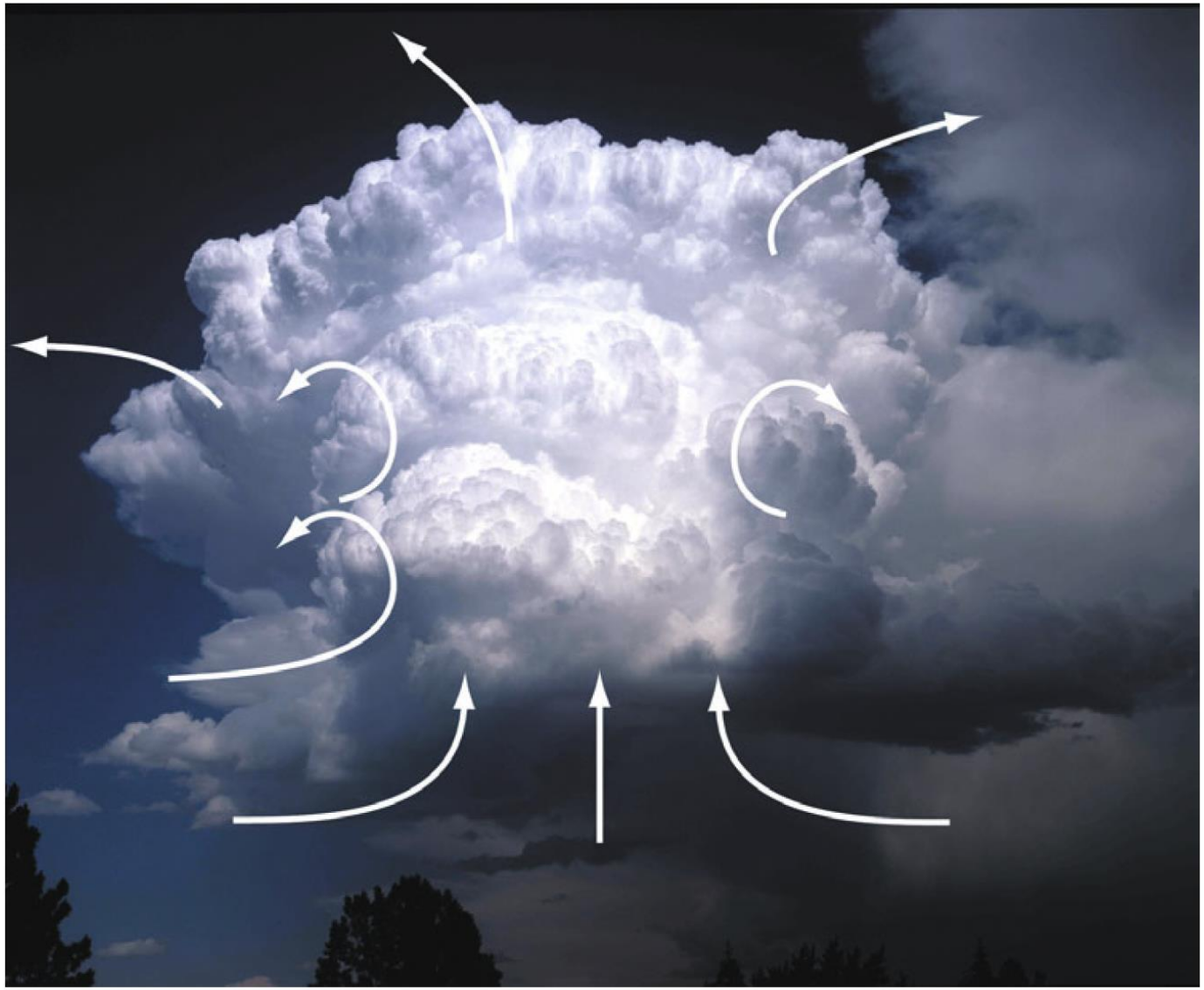

Figure 3.4. Illustration of entrainment of environmental air into a cloud (curled streamlines into curling, rolling, cumulus elements) on July 2, 2011 in Boulder, CO. Air enters the cloud base from below and from the sides. As a result of entrainment, the mass flux of air detraining from the cloud at the top exceeds the mass flux into the cloud base below (photograph by the author).

Figure 3.5. Cumulonimbus anvil on September 9, 2009, in Boulder, CO. Three separate bursts of convection are evident (each burst indicated by an arrow) (photograph by the author).

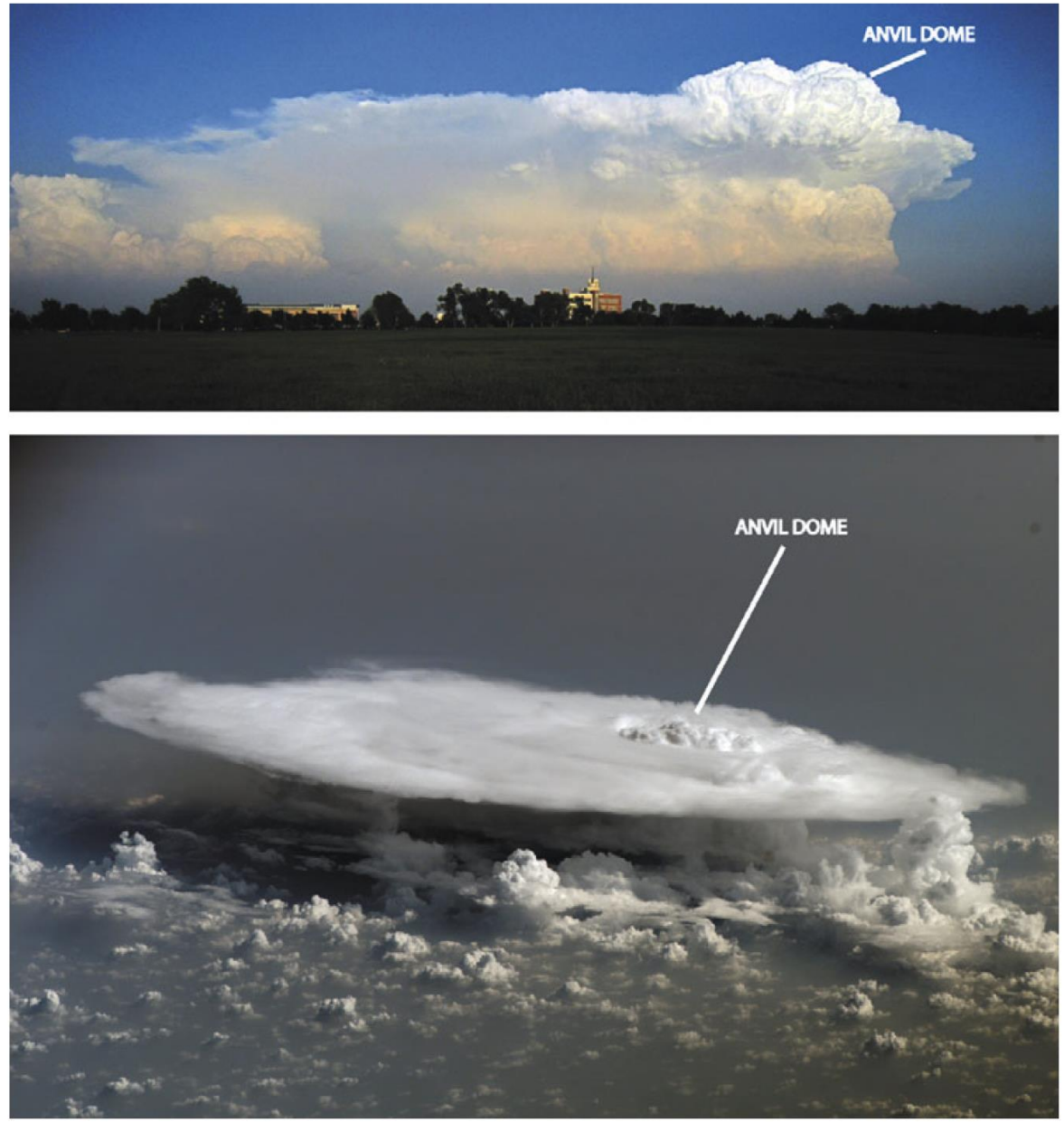

Figure 3.7. Anvil dome (penetrating top) at the top of a convective storm. (top) Tornadic supercell southeast of the National Weather Center, Norman, OK, May 21, 2011 (photograph by the author); (bottom) convective storm viewed from above by International Space Station on February 5, 2008, over Mali in western Africa (from NASA).

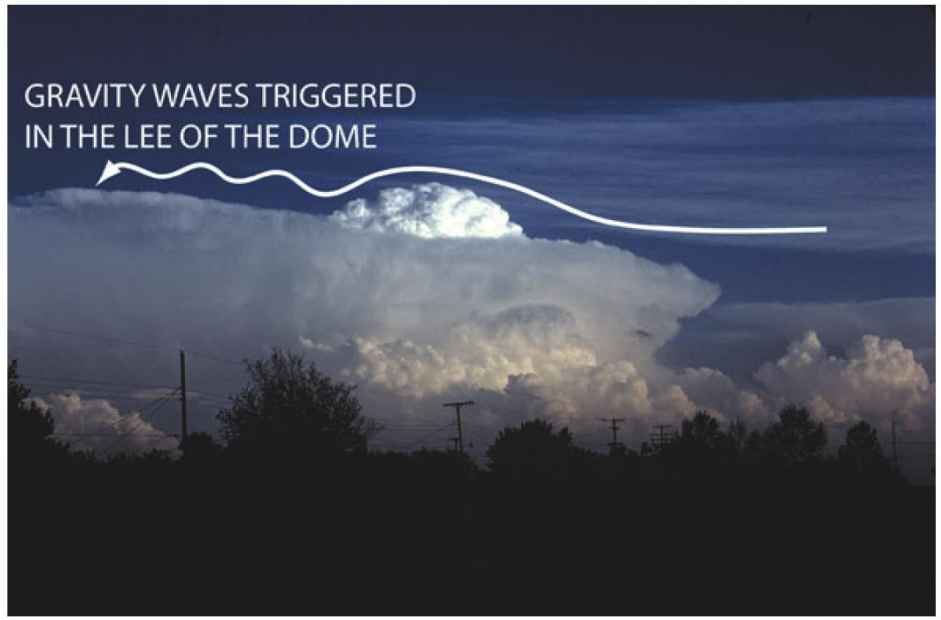

Figure 3.8. Schematic of airflow over a dome at the top of a convective storm in eastern Oklahoma on May 1, 1980. Streamline shown is indicated for flow near the top of the storm when the storm is propagating more slowly than the wind speed. Air is lifted over the dome and then undergoes stable vertical oscillations downstream from the dome (photograph by the author).

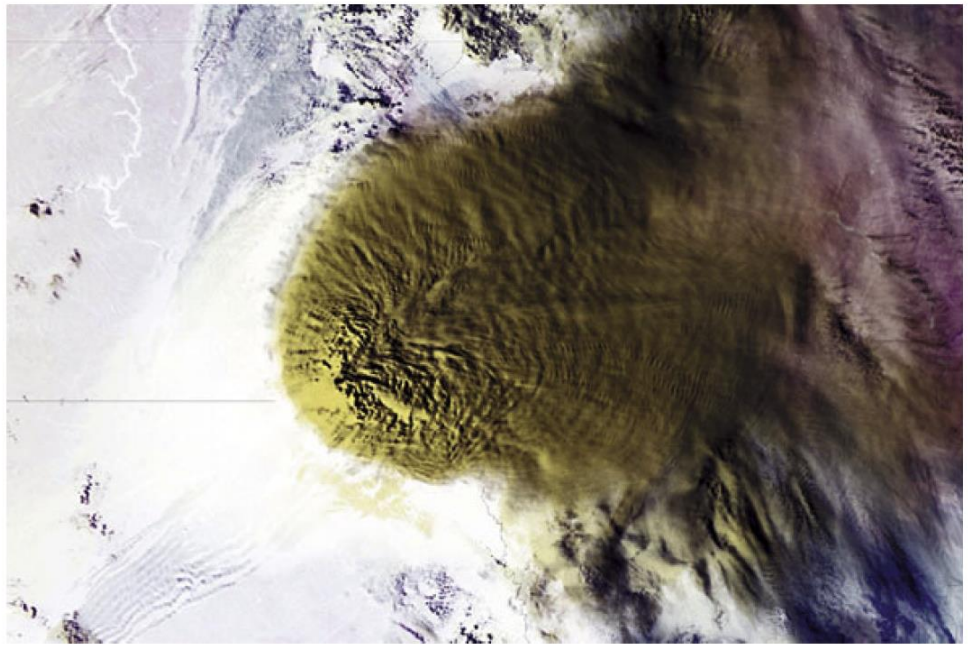

Figure 3.9. Waves in the anvil of a convective storm (caused by gravity waves) on July 9, 2009, over the upper Midwest of the U. S., as seen by the NOAA 15 satellite (from Martin Setvak).

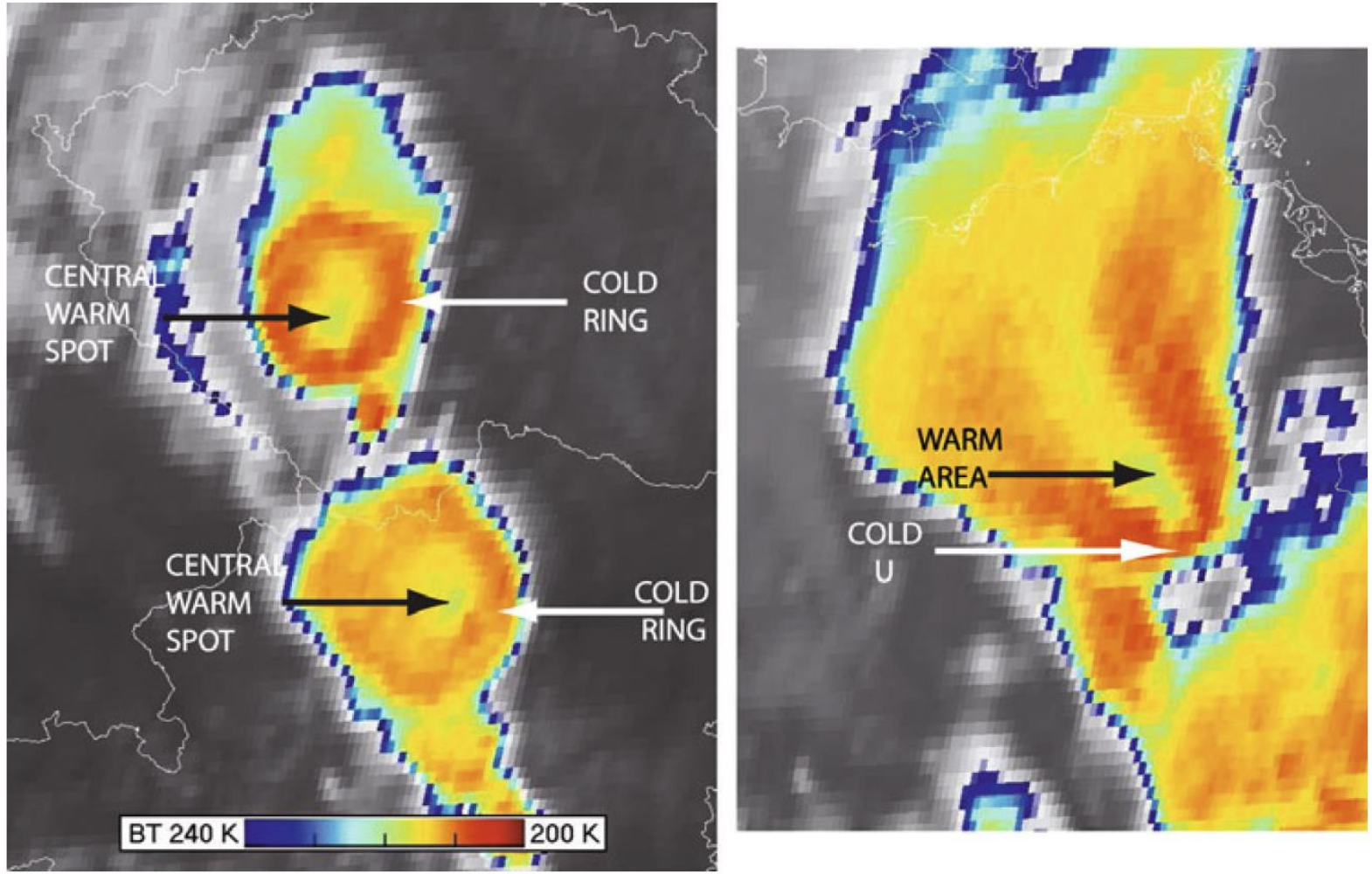

Figure 3.11. Color-enhanced infrared signatures at anvil top. (Left) Cold rings in two convective storms over central Europe as detected by METEOSAT-8. (Right) Cold UV signature in a convective storm over Germany on May 26, 2007, as depicted by METEOSAT-9 (from Martin Setvak).

(a)

(b)

Figure 3.12. (a) Cloud base in a supercell that has striations like an orographic wave cloud, on May 29, 2008, north central Kansas. (b) Orographic wave clouds in the lee of the Rockies just west of Ward, CO on January 2, 2008 (photographs by the author).

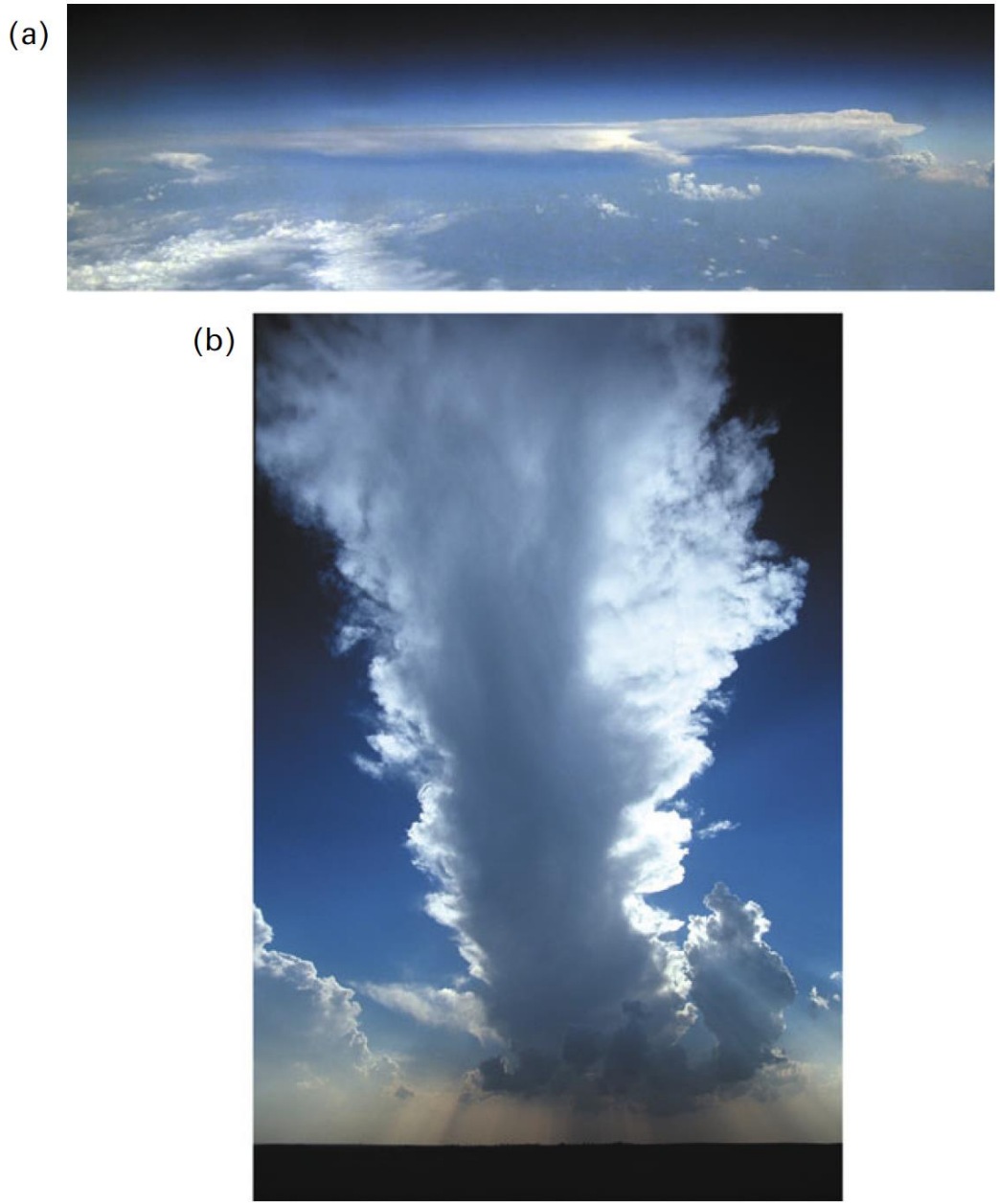

Figure 3.16. Long anvils. (a) Cumulonimbus with a long anvil downstream, as viewed from an aircraft over southwestern Nebraska on July 19, 2009. (b) Developing cumulonimbus in Oklahoma on April 30, 2003 (photographs by the author).

Figure 3.17. Cumulonimbus (developing supercell) with a symmetrical, mushroom-like anvil, on May 26, 1997 in eastern Oklahoma (photograph by the author).

Figure 3.18. Orphan (or "orphaned") anvil on March 15, 2012, Ft. Lauderdale, FL. (Top) Convective storm is dissipating, with precipitation falling; (bottom) anvil has become disconnected from the cloud below and most of the precipitation has ended (photographs by the author).

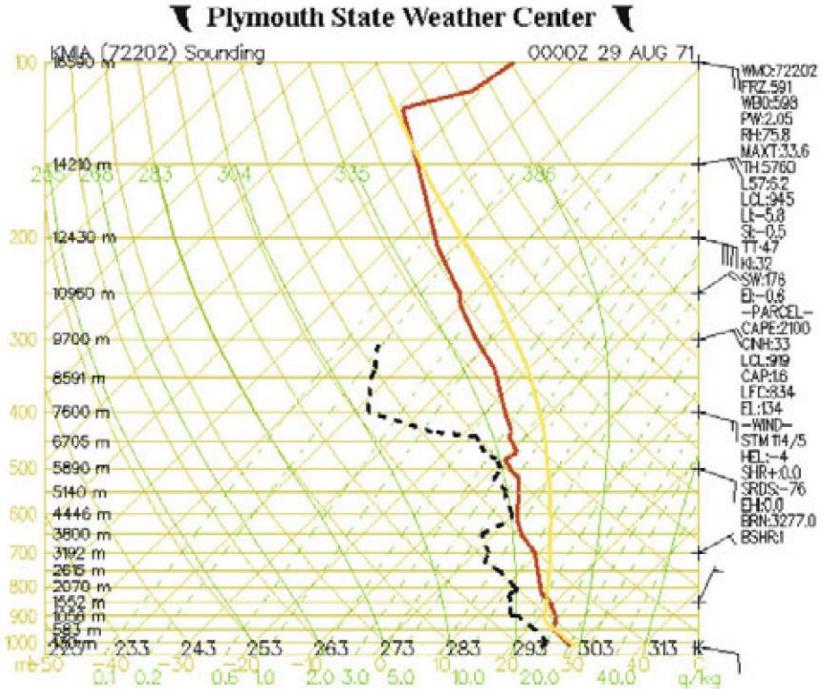

Figure 3.19a. Stages in the life of a Byers–Braham, ordinary-cell convective storm. (Top left) Cumulus congestus stage, on August 28, 1971, over the South Florida peninsula, south of Miami; (top right) cumulus congestus about to hit the tropopause and producing a pileus, on August 28, 1971; (second row, left) mature stage, with an anvil, on August 28, 1971; (second row, right) dissipating stage, off the west coast of South Florida, on August 28, 1973 (photographs by the author). (Bottom) Sounding at Miami, Florida, 00:00 UTC on August 29, 1971, which is a representative environmental sounding for the convective storm on August 28, 1971 (from the Plymouth State College archive and graphics). Vertical shear is weak and CAPE moderate.

Comet sources

https://www.meted.ucar.edu/education_training?query=&page=1

Topic: Convective weather & Radar meteorology

Related to Chapter 1

- Skew-T Mastery
- Principles of Convection II: Using Hodographs
- Radar Signatures for Severe Convective Weather
- Weather Radar Fundamentals
- Principles of Convection I: Buoyancy and CAPE (ucar.edu)

Related to Chapter 2

- Severe Convection: Mesoscale Convective Systems
- An MCS matrix
- Mesoscale Convective Systems: Squall Lines and Bow Echoes
- A Convective Storm Matrix: Buoyancy/Shear Dependencies
- Principles of Convection III: Shear and Convective Storms

建议大家课余看一看